

---

# Efficient Estimation of Average-Case Robustness for Multi-Class Classification

---

Tessa Han\*  
Harvard University  
than@h.harvard.edu

Suraj Srinivas\*  
Harvard University  
ssrinivas@seas.harvard.edu

Himabindu Lakkaraju  
Harvard University  
hlakkaraju@hbs.edu

## Abstract

Robustness in machine learning is commonly studied in the adversarial setting, yet real-world noise (such as measurement noise) is random rather than adversarial. Model behavior under such noise is captured by average-case robustness, i.e., the probability of obtaining consistent predictions in a local region around an input. However, the naïve approach to computing average-case robustness based on Monte-Carlo sampling is statistically inefficient, especially for high-dimensional data, leading to prohibitive computational costs for large-scale applications. In this work, we develop the first analytical estimators to efficiently compute average-case robustness of multi-class discriminative models. These estimators linearize models in the local region around an input and analytically compute the robustness of the resulting linear models. We show empirically that these estimators efficiently compute the robustness of standard deep learning models and demonstrate these estimators’ usefulness for various tasks involving robustness, such as measuring robustness bias and identifying dataset samples that are vulnerable to noise perturbation. In doing so, this work not only proposes a new framework for robustness, but also makes its computation practical, enabling the use of average-case robustness in downstream applications.

notion of robustness is adversarial robustness, the ability of a model to maintain its prediction when presented with adversarial perturbations, i.e., perturbations designed to cause the model to change its prediction. Although adversarial robustness identifies whether a misclassified example exists in a local region around an input, real-world noise (such as measurement noise) is rarely adversarial and often random. The effect of such noise on model predictions is better captured by another notion of robustness: *average-case robustness*, i.e., the fraction of points in a local region around an input for which the model provides consistent predictions. If this fraction is less than one, then an adversarial perturbation exists. In this sense, average-case robustness is a strict generalization of adversarial robustness. Adversarial robustness only detects the presence of a single misclassified instance, a limitation due to its origins in model security. In contrast, average-case robustness offers a more comprehensive view of model behavior. Because we are interested in the applicability of robustness to understand model behavior, help debugging efforts, and improve model generalization via regularization in real-world settings, this paper studies average-case robustness. For convenience, in the rest of this paper we use “average-case robustness” and “local robustness” interchangeably.

In this paper, we take the first steps towards estimating average-case robustness for large-scale multi-class classifiers. We show that the naïve approach to estimating average-case robustness based on Monte-Carlo sampling is statistically inefficient: obtaining an accurate estimate of local robustness using this approach requires a large number of samples from the local region. This inefficiency is exacerbated in the case of high-dimensional data, leading to prohibitive computational costs for large-scale applications. Our work makes the following contributions:

1. We derive novel analytical estimators to efficiently compute the average-case robustness of multi-class classifiers. We also provide estimation error bounds for these estimators that characterizes the

## 1 Introduction

A desirable attribute of machine learning models is robustness to perturbations of input data. One common

errors incurred due to such linearization.

2. We empirically validate these analytical estimators using standard deep learning models and datasets, demonstrating that these estimators accurately and efficiently compute robustness.
3. We demonstrate the usefulness of our analytical estimators for various tasks involving average-case robustness, such as measuring class-level robustness bias (1) (i.e., a model being more locally robust for some classes than for others) and identifying non-robust samples in a dataset.

To our knowledge, this work is the first to investigate average-case robustness for the multi-class setting and develop efficient analytical estimators. In addition, the efficiency of these estimators makes the computation of average-case robustness practical, especially for large deep neural networks.

## 2 Related Work

**Adversarial robustness.** Prior works have proposed methods to generate adversarial attacks (2, 3, 4), which find adversarial perturbations in a local region around a point. In contrast, this work investigates average-case robustness, which calculates the probability that a model’s prediction remains consistent in a local region around a point. Prior works have also proposed methods to certify model robustness (5, 6), providing guarantees of dataset-level robustness (i.e., all points in a dataset are robust to a certain amount of noise). In contrast, this work focuses on establishing point-level local robustness.

**Probabilistic robustness.** Prior works have explored notions of probabilistic and average-case robustness. For instance, (7, 8, 9) focus on certifying robustness of real-valued outputs to input perturbations. In contrast, this work focuses on only those output changes that cause misclassification. Like our work, (10) also considers misclassifications. However, (10) aims to find the smallest neighborhood with no adversarial example, while we compute the probability of misclassification in a given neighborhood. (11, 12) also aim to compute average-case robustness. However, they do so by computing the average loss over the neighborhood, while we use the misclassification rate. Closest to our work is (13) which aims to certify the binary misclassification rate (with respect to a specific class to misclassify to) using lower and upper linear bounds. In contrast, our work estimates the multi-class misclassification rate, as opposed to bounding the quantity in a binary setting. A crucial contribution of our work is its applicability to multi-class classification and the emphasis on estimating, rather than bounding, robustness.

## 3 Average-Case Robustness Estimation

In this section, we first describe the mathematical problem of average-case robustness estimation. Then, we present the naïve estimator based on sampling and derive more efficient analytical estimators.

### 3.1 Notation and Preliminaries

Assume that we have a neural network  $f : \mathbb{R}^d \rightarrow \mathbb{R}^C$  with  $C$  output classes and that the classifier predicts class  $t \in [1, \dots, C]$  for a given input  $\mathbf{x} \in \mathbb{R}^d$ , i.e.,  $t = \arg \max_{i=1}^C f_i(\mathbf{x})$ , where  $f_i$  denotes the logits for the  $i^{\text{th}}$  class. Given this classifier, the average-case robustness estimation problem is to compute the probability of consistent classification (to class  $t$ ) under noise perturbation of the input.

**Definition 1.** We define the *average-case robustness* of a classifier  $f$  to noise  $\mathcal{R}$  at a point  $\mathbf{x}$  as

$$p^{\text{robust}}(\mathbf{x}, t) = P_{\epsilon \sim \mathcal{R}} \left[ \arg \max_i f_i(x + \epsilon) = t \right]$$

Our average-case robustness measure  $p^{\text{robust}}(\mathbf{x}, t)$  is larger the more robust the model is in the local neighborhood around  $\mathbf{x}$ . In this paper, given that robustness is always measured with respect to the predicted class  $t$  at  $\mathbf{x}$ , we henceforth suppress the dependence on  $t$ . We also explicitly show the dependence of  $p^{\text{robust}}$  on the noise scale  $\sigma$  by denoting it as  $p_\sigma^{\text{robust}}$ .

In this work, we shall consider  $\mathcal{R}$  as an isotropic Normal distribution, i.e.,  $\mathcal{R} = \mathcal{N}(0, \sigma^2)$ . However, as we shall discuss in the next section, it is possible to accommodate both non-isotropic and non-Gaussian distributions in our method. Note that for high-dimensional data ( $d \rightarrow \infty$ ), the isotropic Gaussian distribution converges to the uniform distribution on the surface of the sphere with radius  $r = \sigma\sqrt{d}$ <sup>1</sup> due to the concentration of measure phenomenon (14).

Observe that when the domain of the input noise is restricted to an  $\ell_p$  ball,  $p_\sigma^{\text{robust}}$  generalizes the corresponding  $\ell_p$  adversarial robustness. In other words, adversarial robustness is concerned with the quantity  $\mathbf{1}(p_\sigma^{\text{robust}} < 1)$ , i.e., the indicator function that average-case robustness is less than one (which indicates the presence of an adversarial perturbation), while we are concerned with computing the quantity  $p_\sigma^{\text{robust}}$  itself. In the rest of this section, we derive estimators for  $p_\sigma^{\text{robust}}$ .

**The (inefficient) Monte-Carlo estimator.** A naïve estimator of average-case robustness is the Monte-Carlo estimator  $p_\sigma^{\text{mc}}$ . It computes the local robustness

<sup>1</sup>Alternately, if  $\epsilon \sim \mathcal{N}(0, \sigma^2/d)$ , then  $r = \sigma$

of a classifier  $f$  at input  $\mathbf{x}$  by generating  $M$  noisy samples of  $\mathbf{x}$  and then calculating the fraction of these noisy samples that are classified to the same class as  $\mathbf{x}$ . In other words,

$$\begin{aligned} p_\sigma^{\text{robust}}(\mathbf{x}) &= P_{\epsilon \sim \mathcal{N}(0, \sigma^2)} \left[ \arg \max_i f_i(\mathbf{x} + \epsilon) = t \right] \\ &= \mathbb{E}_{\epsilon \sim \mathcal{N}(0, \sigma^2)} \left[ \mathbf{1}_{\arg \max_i f_i(\mathbf{x} + \epsilon) = t} \right] \\ &\approx \frac{1}{M} \sum_{j=1}^M \left[ \mathbf{1}_{\arg \max_i f_i(\mathbf{x} + \epsilon_j) = t} \right] = p_\sigma^{\text{mc}}(\mathbf{x}) \end{aligned}$$

$p_\sigma^{\text{mc}}$  replaces the expectation with the sample average of the  $M$  noisy samples of  $\mathbf{x}$  and has been used in prior work (1). While the estimator errors for the Monte-Carlo estimator are technically independent of dimensionality and is given by  $\mathcal{O}(1/\sqrt{M})$  (14), in practice, for neural networks this requires a large number of random samples to converge to the underlying expectation. For example, for MNIST and CIFAR10 CNNs, it takes around  $M = 10,000$  samples per point for  $p_\sigma^{\text{mc}}$  to converge, which is computationally intensive. Thus, we set out to address this problem by developing more efficient analytical estimators of local robustness.

### 3.2 Robustness Estimation via Linearization

Our goal is to derive computationally efficient estimators of average-case robustness. To this end, we propose to first locally linearize non-linear models and then compute the local robustness of the resulting linear models. This is especially challenging for multi-class classifiers, where the relative orientation of class-wise decision boundaries need to be taken into account to compute local robustness.

Specifically, given a linear model for a three-class classification problem with weights  $w_1, w_2, w_3$  and biases  $b_1, b_2, b_3$ , such that  $y = \arg \max_i \{w_i^\top \mathbf{x} + b_i \mid i \in [1, 2, 3]\}$ , the decision boundary function between classes 1 and 2 is given by  $y_{12} = (w_1 - w_2)^\top \mathbf{x} + (b_1 - b_2)$ . This can be verified as follows: for any  $\mathbf{x}$  such that  $y_{12} = 0$ , we have  $w_1^\top \mathbf{x} + b_1 = w_2^\top \mathbf{x} + b_2$ , making it the decision boundary between classes 1 and 2. If the predicted label at  $\mathbf{x}$  is  $y = 1$ , the relevant quantities are the two pairwise difference terms ( $y_{12}, y_{13}$ ) which characterize the decision boundaries of probable misclassifications into classes 2 and 3 respectively. We take this into account and provide the expression for the linear case below.

**Notation:** For clarity, we represent tensors by collapsing along the ‘class’ dimension, i.e.,  $a_i \Big|_{i=1}^C := (a_1, a_2, \dots, a_i, \dots, a_c)$ , where for an order- $t$  tensor  $a_i$ , the expansion  $a_i \Big|_{i=1}^C$  is an order- $(t+1)$  tensor.

**Lemma 1.** *The local robustness of a multi-class linear model  $f(\mathbf{x}) = \mathbf{w}^\top \mathbf{x} + b$  (with  $\mathbf{w} \in \mathbb{R}^{d \times C}$  and  $b \in \mathbb{R}^C$ ) at point  $\mathbf{x}$  with respect to a target class  $t$  is given by the following. Define weights  $\mathbf{u}_i = \mathbf{w}_t - \mathbf{w}_i \in \mathbb{R}^d, \forall i \neq t$ , where  $\mathbf{w}_t, \mathbf{w}_i$  are rows of  $\mathbf{w}$  and biases  $c_i = \mathbf{u}_i^\top \mathbf{x} + (b_t - b_i) \in \mathbb{R}$ . Then,*

$$\begin{aligned} p_\sigma^{\text{robust}}(\mathbf{x}) &= \Phi_{\mathbf{U}\mathbf{U}^\top} \left( \frac{c_i}{\sigma \|\mathbf{u}_i\|_2} \Big|_{\substack{i=1 \\ i \neq t}}^C \right) \\ \text{where } \mathbf{U} &= \frac{\mathbf{u}_i}{\|\mathbf{u}_i\|_2} \Big|_{\substack{i=1 \\ i \neq t}}^C \in \mathbb{R}^{(C-1) \times d} \end{aligned}$$

and  $\Phi_{\mathbf{U}\mathbf{U}^\top}$  is the  $(C-1)$ -dimensional Normal CDF with zero mean and covariance  $\mathbf{U}\mathbf{U}^\top$ .

*Proof Idea.* The proof involves constructing decision boundary functions  $g_i(\mathbf{x}) = f_t(\mathbf{x}) - f_i(\mathbf{x})$  and computing the probability  $p_\sigma^{\text{robust}}(\mathbf{x}) = P_\epsilon(\bigcup_{i=1, i \neq t}^C g_i(\mathbf{x} + \epsilon) > 0)$ .

For Gaussian  $\epsilon$ , we observe that  $\frac{\mathbf{u}}{\sigma \|\mathbf{u}\|_2}^\top \epsilon \sim \mathcal{N}(0, 1)$  is also a Gaussian, which applied vectorially results in our usage of  $\Phi$ . As convention, we represent  $\mathbf{U}$  in a normalized form to ensure that its rows are unit norm.  $\square$

The proof is in Appendix A.1. The matrix  $\mathbf{U}$  exactly captures the geometry of the linear decision boundaries and the covariance matrix  $\mathbf{U}\mathbf{U}^\top$  encodes the relative similarity between pairs of decision boundaries of different classes.

**Remark.** For the binary classification case, we get  $\mathbf{U}\mathbf{U}^\top = 1$  (a scalar), and  $p_\sigma^{\text{robust}}(\mathbf{x}) = \phi(\frac{c}{\sigma \|\mathbf{u}\|_2})$ , where  $\phi$  is the cdf of the scalar standard normal, which was previously also shown by (13, 15). Hence Lemma 1 is a multi-class generalization of (13, 15).

If the decision boundary vectors  $\mathbf{u}_i$  are all orthogonal to each other, then the covariance matrix  $\mathbf{U}\mathbf{U}^\top$  is identity. However, in practice, we find that the covariance matrix is strongly non-diagonal, indicating that the decision boundaries are not orthogonal to each other. For diagonal covariance matrices, the multivariate Normal CDF (*mvm-cdf*) can be written as the product of univariate Normal CDFs, which is easy to compute. However, the strong non-diagonal nature of covariance matrices in practice leads to the resulting *mvm-cdf* not having a closed form solution, and thus needing to be approximated via sampling (16, 17). However, this sampling is performed in the  $(C-1)$ -dimensional space as opposed to the  $d$ -dimensional space that  $p_\sigma^{\text{mc}}$  samples from. In practice, for classification problems, we often have  $C \ll d$ , making sampling in  $(C-1)$ -dimensions more efficient. We now discuss the applicability of this solution to non-Gaussian noise.

**Lemma 2. (Application to non-Gaussian noise)** For high-dimensional data ( $d \rightarrow \infty$ ), Lemma 1 generalizes to any coordinate-wise independent noise distribution that satisfies Lyapunov’s condition.

*Proof Idea.* Applying Lyapunov’s central limit theorem (18), given  $\epsilon \sim \mathcal{R}$  is sampled from some distribution  $\mathcal{R}$ , we have  $\frac{\mathbf{u}}{\sigma\|\mathbf{u}\|_2}^\top \epsilon = \sum_{j=1}^d \frac{\mathbf{u}_j}{\sigma\|\mathbf{u}\|_2} \epsilon_j \xrightarrow{d} \mathcal{N}(0, 1)$ , which holds as long as the sequence  $\{\frac{\mathbf{u}_j}{\|\mathbf{u}\|_2} \epsilon_j\}$  are independent random variables and satisfy the Lyapunov condition, which encodes the fact that higher-order moments of such distributions progressively shrink.  $\square$

Thus, as long as the input noise distribution is “well-behaved”, the central limit theorem ensures that the distribution of high-dimensional dot products is Gaussian, thus motivating our use of the *mvn-cdf* more generally beyond Gaussian input perturbations. We note that it is also possible to easily generalize Lemma 1 to **non-isotropic** Gaussian perturbations with a covariance matrix  $\mathcal{C}$ , which only changes the form of the covariance matrix of the *mvn-cdf* from  $\mathbf{U}\mathbf{U}^\top \rightarrow \mathbf{U}\mathcal{C}\mathbf{U}^\top$ , which we elaborate in Appendix A.1. In the rest of this paper, we focus on the isotropic case.

### 3.2.1 Estimator 1: The Taylor Estimator

Using the estimator derived for multi-class linear models in Lemma 1, we now derive the Taylor estimator, a local robustness estimator for non-linear models.

**Proposition 1.** *The Taylor estimator for the local robustness of a classifier  $f$  at point  $\mathbf{x}$  with respect to target class  $t$  is given by linearizing  $f$  around  $\mathbf{x}$  using a first-order Taylor expansion, with decision boundaries  $g_i(\mathbf{x}) = f_t(\mathbf{x}) - f_i(\mathbf{x})$ ,  $\forall i \neq t$ , leading to*

$$p_\sigma^{\text{taylor}}(\mathbf{x}) = \Phi_{\mathbf{U}\mathbf{U}^\top} \left( \frac{g_i(\mathbf{x})}{\sigma\|\nabla_{\mathbf{x}}g_i(\mathbf{x})\|_2} \Big|_{\substack{i=1 \\ i \neq t}}^C \right)$$

with  $\mathbf{U}$  and  $\Phi$  defined as in the linear case.

The proof is in Appendix A.1. It involves locally linearizing non-linear decision boundary functions  $g_i(\mathbf{x})$  using a Taylor series expansion. We expect this estimator to have a small error when the underlying model is well-approximated by a locally linear function in the local neighborhood. We formalize this intuition by computing the estimation error for a quadratic classifier.

**Proposition 2.** *The estimation error of the Taylor estimator for a classifier with a quadratic decision boundary  $g_i(\mathbf{x}) = \mathbf{x}^\top A_i \mathbf{x} + \mathbf{u}_i^\top \mathbf{x} + c_i$  and positive-semidefinite  $A_i$  is upper bounded by*

$$|p_\sigma^{\text{robust}}(\mathbf{x}) - p_\sigma^{\text{taylor}}(\mathbf{x})| \leq k\sigma^{C-1} \prod_{\substack{i=1 \\ i \neq t}}^C \frac{\lambda_{\max}^{A_i}}{\|\mathbf{u}_i\|_2}$$

for noise  $\epsilon \sim \mathcal{N}(0, \sigma^2/d)$ , in the limit of  $d \rightarrow \infty$ . Here,  $\lambda_{\max}^{A_i}$  is the max eigenvalue of  $A_i$ , and  $k$  is a small problem dependent constant.

The proof is in Appendix A.1. This statement formalizes two key intuitions with regards to the Taylor estimator: (1) the estimation error depends on the size of the local neighborhood  $\sigma$  (the smaller the local neighborhood, the more locally linear the model, and the smaller the estimator error), and (2) the estimation error depends on the extent of non-linearity of the underlying function, which is given by the ratio of the max eigenvalue of  $A$  to the Frobenius norm of the linear term. This measure of non-linearity of a function, called normalized curvature, has also been independently proposed by previous work (19). Notably, if the max eigenvalue is zero, then the function  $g_i(\mathbf{x})$  is exactly linear, and the estimation error is zero.

### 3.2.2 Estimator 2: The MMSE Estimator

While the Taylor estimator is more efficient than the naïve one, it has a drawback: its linearization is only faithful at points near the data point and not necessarily at the noisy points. To partly fix this issue, we use a linearization that is faithful to the model over the entire noise distribution, not just near the data point. Linearization has been studied in feature attribution research, which concerns itself with approximating non-linear models with linear ones to produce model explanations (20). In particular, the SmoothGrad (21) technique has been described as the MMSE (minimum mean-squared error) optimal linearization of the model (20, 22) in a Gaussian neighborhood around the data point. Using a similar technique, we propose the MMSE estimator  $p_\sigma^{\text{mmse}}$  as follows.

**Proposition 3.** *The MMSE estimator for the local robustness of a classifier  $f$  at point  $\mathbf{x}$  with respect to target class  $t$  is given by an MMSE linearization  $f$  around  $\mathbf{x}$ , for decision boundaries  $g_i(\mathbf{x}) = f_t(\mathbf{x}) - f_i(\mathbf{x})$ ,  $\forall i \neq t$ , leading to*

$$p_\sigma^{\text{mmse}}(\mathbf{x}) = \Phi_{\mathbf{U}\mathbf{U}^\top} \left( \frac{\tilde{g}_i(\mathbf{x})}{\sigma\|\nabla_{\mathbf{x}}\tilde{g}_i(\mathbf{x})\|_2} \Big|_{\substack{i=1 \\ i \neq t}}^C \right)$$

$$\text{where } \tilde{g}_i(\mathbf{x}) = \frac{1}{N} \sum_{j=1}^N g_i(\mathbf{x} + \epsilon), \quad \epsilon \sim \mathcal{N}(0, \sigma^2)$$

with  $\mathbf{U}$  and  $\Phi$  defined as in the linear case, and  $N$  is the number of perturbations.

The proof is in Appendix A.1. It involves creating a randomized smooth model (5) from the base model and computing the decision boundaries of this smooth model. We show, for the first time, that performing

such randomization helps compute robustness information for the original base model. We now compute the estimation error of the MMSE estimator.

**Proposition 4.** *The estimation error of the MMSE estimator for a classifier with a quadratic decision boundary  $g_i(\mathbf{x}) = \mathbf{x}^\top A_i \mathbf{x} + \mathbf{u}_i^\top \mathbf{x} + c_i$  and positive-semidefinite  $A_i$  is upper bounded by*

$$|p_\sigma^{\text{robust}}(\mathbf{x}) - p_\sigma^{\text{mmse}}(\mathbf{x})| \leq k\sigma^{C-1} \prod_{\substack{i=1 \\ i \neq t}}^C \frac{\lambda_{\max}^{A_i} - \lambda_{\text{mean}}^{A_i}}{\|\mathbf{u}_i\|_2}$$

for noise  $\epsilon \sim \mathcal{N}(0, \sigma^2/d)$ , in the limit of  $d \rightarrow \infty$  and  $N \rightarrow \infty$ . Here,  $\lambda_{\max}^{A_i}, \lambda_{\text{mean}}^{A_i}$  are the maximum and mean eigenvalue of  $A_i$  respectively, and  $k$  is a small problem dependent constant.

The proof is in Appendix A.1. The result above highlights two aspects of the MMSE estimator: (1) it incurs a smaller estimation error than the Taylor estimator, and (2) even in the limit of large number of samples  $N \rightarrow \infty$ , the error of the MMSE estimator is non-zero, except when  $\lambda_{\text{mean}}^{A_i} = \lambda_{\max}^{A_i}$ . For PSD matrices, this implies that  $A_i$  is a multiple of the identity.<sup>2</sup>

### 3.2.3 Approximating $\Phi$

One drawback of the Taylor and MMSE estimators is their use of the *mvn-cdf*, which does not have a closed form solution and can cause the estimators to be slow for settings with a large number of classes  $C$ . In addition, the *mvn-cdf* makes these estimators non-differentiable, which is inconvenient for applications which require differentiating  $p_\sigma^{\text{robust}}$ . To alleviate these issues, we wish to approximate the *mvn-cdf* with an analytical closed-form expression. As CDFs are monotonically increasing functions, the approximation should also be monotonically increasing.

To this end, it has been previously shown that the *univariate* Normal CDF  $\phi$  is well-approximated by the sigmoid function (23). It is also known that when  $\mathbf{U}\mathbf{U}^\top = I$ , *mvn-cdf* is given by  $\Phi(\mathbf{x}) = \prod_i \phi(\mathbf{x}_i)$ , i.e., it is given by the product of the univariate normal CDFs. Thus, we may choose to approximate  $\Phi(\mathbf{x}) = \prod_i \text{sigmoid}(\mathbf{x})$ . However, when the inputs are small, this can be simplified as follows:

$$\begin{aligned} \Phi_I(\mathbf{x}) &= \prod_i \phi(\mathbf{x}_i) \approx \prod_i \frac{1}{1 + \exp(-\mathbf{x}_i)} \quad (\text{see (23)}) \\ &= \frac{1}{1 + \sum_i \exp(-\mathbf{x}_i) + \sum_{j,k} \exp(-\mathbf{x}_j - \mathbf{x}_k) + \dots} \\ &\approx \frac{1}{1 + \sum_i \exp(-\mathbf{x}_i)} \quad (\text{for } \mathbf{x}_i \rightarrow \infty \forall i) \end{aligned}$$

We call the final expression the “multivariate sigmoid” (*mv-sigmoid*) which serves as our approximation of *mvn-cdf*, especially at the tails of the distribution. While we expect estimators using *mv-sigmoid* to approximate ones using *mvn-cdf* only when  $\mathbf{U}\mathbf{U}^\top = \mathbf{I}$ , we find experimentally that the approximation works well even for practical values of the covariance matrix  $\mathbf{U}\mathbf{U}^\top$ . Using this approximation to substitute *mv-sigmoid* for *mvn-cdf* in the  $p_\sigma^{\text{taylor}}$  and  $p_\sigma^{\text{mmse}}$  estimators yields the  $p_\sigma^{\text{taylor\_mvs}}$  and  $p_\sigma^{\text{mmse\_mvs}}$  estimators, respectively.

**Relationship with Softmax.** A common method to estimate the confidence of model predictions is to use the softmax function applied to the logits  $f_i(\mathbf{x})$  of a model. We note that softmax is identical to *mv-sigmoid* when directly applied to the logits of neural networks:

$$\begin{aligned} \text{softmax}_t \left( f_i(\mathbf{x}) \Big|_{i=1}^C \right) &= \frac{\exp(f_t(\mathbf{x}))}{\sum_{i=1}^C \exp(f_i(\mathbf{x}))} = \\ &= \frac{1}{1 + \sum_{\substack{i=1 \\ i \neq t}}^C \exp(f_i(\mathbf{x}) - f_t(\mathbf{x}))} = \text{mv-sigmoid} \left( g_i(\mathbf{x}) \Big|_{\substack{i=1 \\ i \neq t}}^C \right) \end{aligned}$$

Recall that  $g_i(\mathbf{x}) = f_t(\mathbf{x}) - f_i(\mathbf{x})$  is the decision boundary function. Note that this equivalence only holds for the specific case of logits. Comparing the expressions of softmax applied to logits above and the Taylor estimator, we notice that they are only different in that the Taylor estimator divides by the gradient norm, and uses the *mvn-cdf* function instead of *mv-sigmoid*. Given this similarity to the Taylor estimator, it is reasonable to ask whether softmax applied to logits (henceforth  $p_T^{\text{softmax}}$  for softmax with temperature  $T$ ) itself can be a “good enough” estimator of  $p_\sigma^{\text{robust}}$  in practice. In other words, does  $p_T^{\text{softmax}}$  well-approximate  $p_\sigma^{\text{robust}}$  in certain settings?

In general, this cannot hold because softmax does not take in information about  $\mathbf{U}\mathbf{U}^\top$ , nor does it use the gradient information used in all of our estimators, although the temperature parameter  $T$  can serve as a substitute for  $\sigma$  in our expressions. In Appendix A.1, we provide a theoretical result for a restricted linear setting where softmax can indeed match the behavior of  $p_\sigma^{\text{taylor\_mvs}}$ ,

<sup>2</sup>When  $d \rightarrow \infty$ ,  $\epsilon^\top A \epsilon = \lambda \|\epsilon\|^2 = \lambda \sigma^2$  is a constant, and thus an isotropic quadratic function resembles a linear one in this neighborhood.

which happens precisely when  $\mathbf{U}\mathbf{U}^\top = \mathbf{I}$  and all the class-wise gradients are equal. In the next section, we demonstrate empirically that the softmax estimator  $p_T^{\text{softmax}}$  is a poor estimator of average robustness in practice.

## 4 Empirical Evaluation

In this section, we first evaluate the estimation errors and computational efficiency of the analytical estimators, and then evaluate the impact of robustness training within models on these estimation errors. Then, we analyze the relationship between average-case robustness and softmax probability. Lastly, we demonstrate the usefulness of local robustness and its analytical estimators in real-world applications. Key results are discussed in this section and full results are in Appendix A.4.

**Datasets and models.** We evaluate the estimators on four datasets: MNIST (24), FashionMNIST (25), CIFAR10 (26), and CIFAR100 (26). For MNIST and FashionMNIST, we train linear models and CNNs to perform classification. For CIFAR10 and CIFAR100, we train ResNet18 (27) models to perform classification. We train the ResNet18 models using varying levels of gradient norm regularization ( $\lambda$ ) to obtain models with varying levels of robustness. The experiments below use each dataset’s full test set, each consisting of 10,000 points. Additional details about the datasets and models are described in Appendix A.2 and A.3.

### 4.1 Evaluation of the estimation errors of analytical estimators

To empirically evaluate the estimation error of our estimators, we calculate  $p_\sigma^{\text{robust}}$  for each model using  $p_\sigma^{\text{mc}}$ ,  $p_\sigma^{\text{taylor}}$ ,  $p_\sigma^{\text{mmse}}$ ,  $p_\sigma^{\text{taylor\_mvs}}$ ,  $p_\sigma^{\text{mmse\_mvs}}$ , and  $p_T^{\text{softmax}}$  for different  $\sigma$  values. For  $p_\sigma^{\text{mc}}$ ,  $p_\sigma^{\text{mmse}}$ , and  $p_\sigma^{\text{mmse\_mvs}}$ , we use a sample size at which these estimators have converged ( $n = 10000, 500,$  and  $500$ , respectively). (Convergence analyses are in Appendix A.4.) We take the monte-carlo estimator as the gold standard estimate of  $p_\sigma^{\text{robust}}$ , and compute the absolute and relative difference between  $p_\sigma^{\text{mc}}$  and the other estimators to evaluate their estimation errors.

The performance of the estimators for the FashionMNIST CNN model is shown in Figure 1a. The results indicate that  $p_\sigma^{\text{mmse\_mvs}}$  and  $p_\sigma^{\text{mmse}}$  are the best estimators of  $p_\sigma^{\text{robust}}$ , followed closely by  $p_\sigma^{\text{taylor\_mvs}}$  and  $p_\sigma^{\text{taylor}}$ , trailed by  $p_T^{\text{softmax}}$ . This is consistent with the theory in Section 3, where the analytical estimation errors of  $p_\sigma^{\text{mmse}}$  are lower than  $p_\sigma^{\text{taylor}}$ .

The results also confirm that the smaller the noise

neighborhood  $\sigma$ , the more accurately the estimators compute  $p_\sigma^{\text{robust}}$ . For the MMSE and Taylor estimators, this is because their linear approximation of the model around the input is more faithful for smaller  $\sigma$ . As expected, when the model is linear,  $p_\sigma^{\text{taylor}}$  and  $p_\sigma^{\text{mmse}}$  accurately compute  $p_\sigma^{\text{robust}}$  for all  $\sigma$ ’s (Appendix A.4). For the softmax estimator,  $p_T^{\text{softmax}}$  values are constant over  $\sigma$  and this particular model has high  $p_T^{\text{softmax}}$  values for most points. Thus, for small  $\sigma$ ’s where  $p_\sigma^{\text{robust}}$  is near one,  $p_T^{\text{softmax}}$  happens to approximate  $p_\sigma^{\text{robust}}$  for this model. Examples of images with varying levels of noise ( $\sigma$ ) are in Appendix A.4.

### Impact of robust training on estimation errors.

The performance of  $p_\sigma^{\text{mmse}}$  for CIFAR10 ResNet18 models of varying levels of robustness is shown in Figure 1b. The results indicate that for more robust models (larger  $\lambda$ ), the estimator is more accurate over a larger  $\sigma$ . This is because gradient norm regularization leads to models that are more locally linear (19), making the estimator’s linear approximation of the model around the input more accurate over a larger  $\sigma$ , making its  $p_\sigma^{\text{robust}}$  values more accurate.

### Evaluating estimation error of mv-sigmoid.

To examine *mv-sigmoid*’s approximation of *mvn-cdf*, we compute both functions using the same inputs ( $z = \frac{g_i(\mathbf{x})}{\sigma \|\nabla_{\mathbf{x}} g_i(\mathbf{x})\|_2} \Big|_{i=1, \dots, C, i \neq t}$ , as described in Proposition 1) for the CIFAR10 ResNet18 model for different  $\sigma$ . The plot of *mv-sigmoid*( $z$ ) against *mvn-cdf*( $z$ ) for  $\sigma = 0.05$  is shown in Figure 2. The results indicate that the two functions are strongly positively correlated with low approximation error, suggesting that *mv-sigmoid* approximates the *mvn-cdf* well in practice.

Estimator	# samples ( $n$ )	CPU runtime (h:m:s)	GPU Runtime (h:m:s)
$p_\sigma^{\text{mc}}$	$n = 10000$	1:41:11	0:19:56
$p_\sigma^{\text{taylor}}$	N/A	0:00:08	0:00:02
$p_\sigma^{\text{mmse}}$	$n = 5$	0:00:41	0:00:06

Table 1: Runtimes of  $p_\sigma^{\text{robust}}$  estimators. Each estimator computes  $p_{\sigma=0.1}^{\text{robust}}$  for the CIFAR10 ResNet18 model for 50 data points. Estimators that use sampling use the minimum number of samples necessary for convergence. Runtimes are in the format of hour:minute:second. The GPU used was a Tesla V100. The analytical estimators ( $p_\sigma^{\text{taylor}}$  and  $p_\sigma^{\text{mmse}}$ ) are more efficient than the naïve estimator ( $p_\sigma^{\text{mc}}$ ).

### 4.2 Evaluation of computational efficiency of analytical estimators

We examine the efficiency of the estimators by measuring their runtimes when calculating  $p_{\sigma=0.1}^{\text{robust}}$  for the

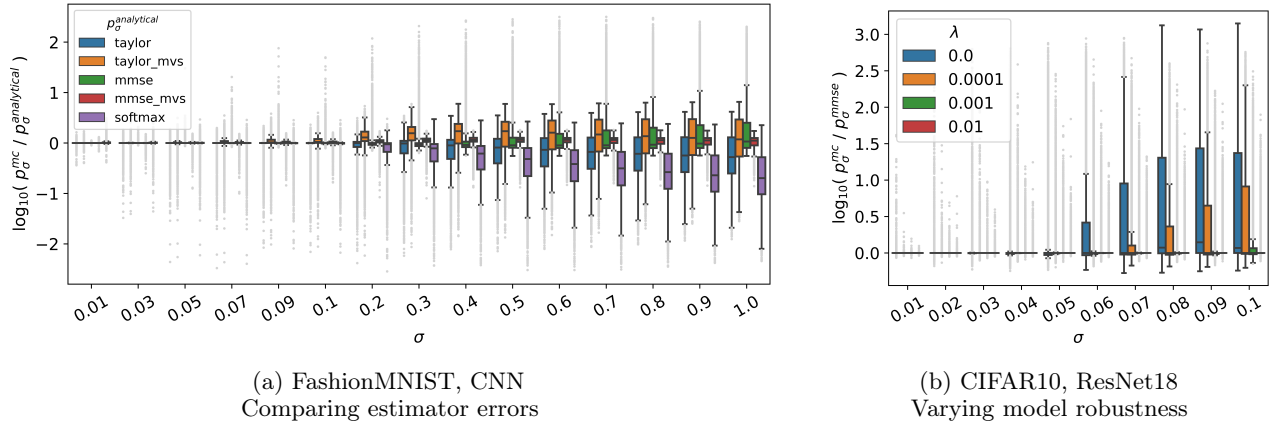


Figure 1: Empirical evaluation of analytical estimators. (a) The smaller the noise neighborhood  $\sigma$ , the more accurately the estimators compute  $p_\sigma^{\text{robust}}$ .  $p_\sigma^{\text{mmse}}$  and  $p_\sigma^{\text{mmse\_mvs}}$  are the best estimators of  $p_\sigma^{\text{robust}}$ , followed closely by  $p_\sigma^{\text{taylor\_mvs}}$  and  $p_\sigma^{\text{taylor}}$ , trailed by  $p_T^{\text{softmax}}$ . (b) For more robust models, the estimators compute  $p_\sigma^{\text{robust}}$  more accurately over a larger  $\sigma$ . Together, these results indicate that the analytical estimators accurately compute  $p_\sigma^{\text{robust}}$ .

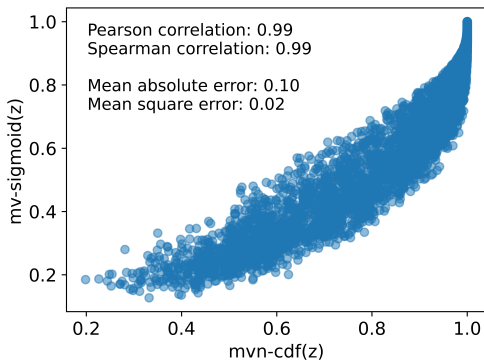


Figure 2: Correlation of  $mvn\text{-cdf}(z)$  and  $mv\text{-sigmoid}(z)$  for the CIFAR10 ResNet18 model. The formulation of  $z$  is described in Section 4.1. In practice,  $mv\text{-sigmoid}$  approximates  $mvn\text{-cdf}$  well.

CIFAR10 ResNet18 model for 50 points. Runtimes are displayed in Table 1. They indicate that  $p_\sigma^{\text{taylor}}$  and  $p_\sigma^{\text{mmse}}$  perform 35x and 17x faster than  $p_\sigma^{\text{mc}}$ , respectively. Additional runtimes are in Appendix A.4.

### 4.3 Softmax probability is not a good proxy for average-case robustness

To examine the relationship between  $p_\sigma^{\text{robust}}$  and  $p_T^{\text{softmax}}$ , we calculate  $p_\sigma^{\text{mmse}}$  and  $p_T^{\text{softmax}}$  for CIFAR10 and CIFAR100 models of varying levels of robustness, and measure the correlation of their values and ranks using Pearson and Spearman correlations. Results are in Figure 3. For a non-robust model,  $p_\sigma^{\text{robust}}$  and  $p_T^{\text{softmax}}$  are not strongly correlated (Figure 3a). As model robustness increases, the two quantities become

more correlated (Figures 3b and 3c). However, even for robust models, the relationship between the two quantities is mild (Figure 3c). That  $p_\sigma^{\text{robust}}$  and  $p_T^{\text{softmax}}$  are not strongly correlated is consistent with the theory in Section 3: in general settings,  $p_T^{\text{softmax}}$  is not a good estimator for  $p_\sigma^{\text{robust}}$ .

### 4.4 Applications of average-case robustness

#### Detecting robustness bias among classes: Is the model differently robust for different classes?

We demonstrate that  $p_\sigma^{\text{robust}}$  can detect bias in local robustness by examining its distribution for each class for each model and test set over different  $\sigma$ 's. Results for the CIFAR10 ResNet18 model are in plotted in Figure 4. The results show that different classes have different  $p_\sigma^{\text{robust}}$  distributions, i.e., the model is more locally robust for some classes (e.g., frog) than for others (e.g., airplane). The results also show that  $p_\sigma^{\text{mc}}$  and  $p_\sigma^{\text{mmse}}$  have very similar distributions, further indicating that the latter well-approximates the former. Thus,  $p_\sigma^{\text{robust}}$  can be applied to detect robustness bias among classes, which is critical when models are deployed in high-stakes, real-world settings.

**Identifying non-robust dataset samples.** While robustness is typically viewed as the property of a model, the average-case robustness perspective compels us to view robustness as a joint property of both the model and the data point. In light of this, we can ask, given the same model, which samples are robustly and non-robustly classified? We evaluate whether  $p_\sigma^{\text{robust}}$  can distinguish such images better than  $p_T^{\text{softmax}}$ . To this end, we train a simple CNN to distinguish between images with high and low  $p_\sigma^{\text{mmse}}$  and the same CNN to also

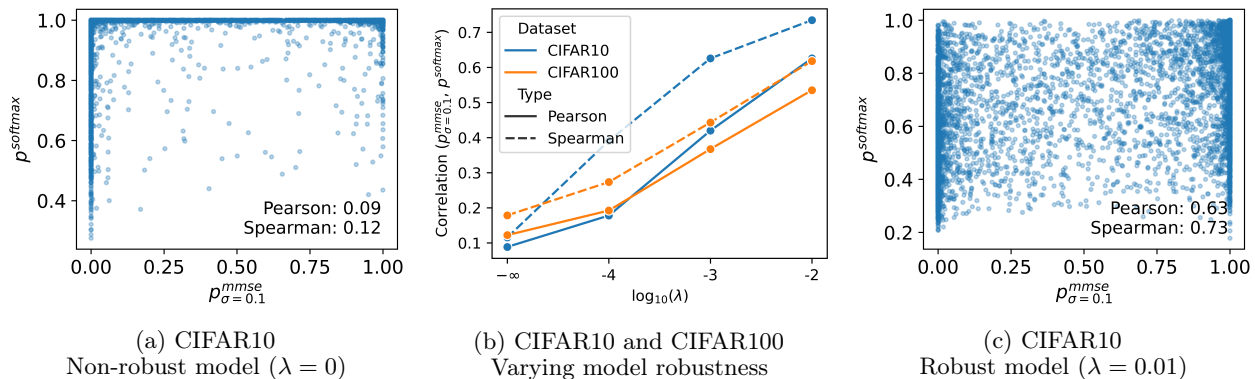


Figure 3: Relationship between  $p_\sigma^{\text{robust}}$  and  $p_T^{\text{softmax}}$  for CIFAR10 and CIFAR100 ResNet18 models. (a) For a non-robust model,  $p_\sigma^{\text{robust}}$  and  $p_T^{\text{softmax}}$  are not strongly correlated. (b) As model robustness increases, the two quantities become more correlated. (c) However, even for robust models, the relationship between  $p_\sigma^{\text{robust}}$  and  $p_T^{\text{softmax}}$  is mild. Together, these results indicate that, consistent with the theory in Section 3,  $p_T^{\text{softmax}}$  is not a good estimator for  $p_\sigma^{\text{robust}}$  in general settings.

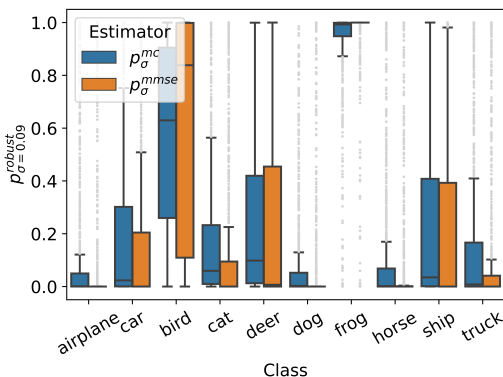


Figure 4: Local robustness bias among classes for the ResNet18 CIFAR10 model.  $p_\sigma^{\text{robust}}$  reveals that the model is less locally robust for some classes than for others. The analytical estimator  $p_\sigma^{\text{mmse}}$  properly captures this model bias.

distinguish between images with high and low  $p_T^{\text{softmax}}$  (additional setup details described in Appendix A.4). Then, we compare the performance of the two models. For CIFAR10, the test set accuracy for the  $p_\sigma^{\text{mmse}}$  CNN is **92%** while that for the  $p_T^{\text{softmax}}$  CNN is **58%**. These results indicate that  $p_\sigma^{\text{robust}}$  better identifies images that are robust to and vulnerable to random noise than  $p_T^{\text{softmax}}$ .

We also present visualizations of images with the highest and lowest  $p_\sigma^{\text{mmse}}$  in each class for each model. For comparison, we do the same with  $p_T^{\text{softmax}}$ . Example CIFAR10 images are shown in the Appendix A.4. We observe that images with low  $p_\sigma^{\text{robust}}$  tend to have neutral colors, with the object being a similar color as the background (making the prediction likely to change when the image is slightly perturbed), while images

with high  $p_\sigma^{\text{robust}}$  tend to be brightly-colored, with the object strongly contrasting with the background (making the prediction likely to stay constant when the image is slightly perturbed). These differences are not as evident for images with the highest and lowest  $p_T^{\text{softmax}}$ . Overall, these results showcase the potential of local robustness in identifying non-robust dataset samples more reliably than softmax probabilities.

## 5 Conclusion

In this work, we take the first steps towards estimating average-case robustness of multi-class classifiers. Studying average-case robustness provides several advantages over adversarial robustness. First, the nature of real-world noise demands randomized average-case analysis rather than an adversarial one. Second, average-case robustness strictly generalizes adversarial robustness, and therefore provides more information about model behavior than adversarial robustness. Finally, we believe that average-case robustness can offer a gentler objective to train neural networks, when compared to the adversarial case. In particular, requiring models to minimize the probability of misclassification in a local neighborhood is a more lenient objective than attempting to eliminate misclassification entirely as is usually done in adversarial robustness (28).

Future research directions include exploring additional applications of local robustness, such as training average-case robust models that minimize the probability of misclassification and using average-case robustness as a measure of prediction uncertainty.

## References

- [1] Vedant Nanda, Samuel Dooley, Sahil Singla, Soheil Feizi, and John P Dickerson. Fairness through robustness: Investigating robustness disparity in deep learning. *ACM Conference on Fairness, Accountability, and Transparency*, 2021.
- [2] Nicholas Carlini and David Wagner. Towards evaluating the robustness of neural networks. *IEEE Symposium on Security and Privacy*, 2017.
- [3] Ian J Goodfellow, Jonathon Shlens, and Christian Szegedy. Explaining and harnessing adversarial examples. *International Conference on Learning Representations*, 2015.
- [4] Seyed-Mohsen Moosavi-Dezfooli, Alhussein Fawzi, and Pascal Frossard. DeepFool: A simple and accurate method to fool deep neural networks. *IEEE Conference on Computer Vision and Pattern Recognition*, 2016.
- [5] Jeremy Cohen, Elan Rosenfeld, and Zico Kolter. Certified adversarial robustness via randomized smoothing. *International Conference on Machine Learning*, 2019.
- [6] Nicholas Carlini, Florian Tramer, Krishnamurthy Dvijotham, Leslie Rice, Mingjie Sun, and Zico Kolter. (Certified!!) adversarial robustness for free! *International Conference on Learning Representations*, 2022.
- [7] Mahyar Fazlyab, Manfred Morari, and George J Pappas. Probabilistic verification and reachability analysis of neural networks via semidefinite programming. In *2019 IEEE 58th Conference on Decision and Control (CDC)*, pages 2726–2731. IEEE, 2019.
- [8] Aounon Kumar, Alexander Levine, Soheil Feizi, and Tom Goldstein. Certifying confidence via randomized smoothing. *Advances in Neural Information Processing Systems*, 33:5165–5177, 2020.
- [9] Ravi Mangal, Aditya V Nori, and Alessandro Orso. Robustness of neural networks: A probabilistic and practical approach. In *2019 IEEE/ACM 41st International Conference on Software Engineering: New Ideas and Emerging Results (ICSE-NIER)*, pages 93–96. IEEE, 2019.
- [10] Jean-Yves Franceschi, Alhussein Fawzi, and Omar Fawzi. Robustness of classifiers to uniform lp and gaussian noise. In *International Conference on Artificial Intelligence and Statistics*, pages 1280–1288. PMLR, 2018.
- [11] Alexander Robey, Luiz Chamon, George J Pappas, and Hamed Hassani. Probabilistically robust learning: Balancing average and worst-case performance. In *International Conference on Machine Learning*, pages 18667–18686. PMLR, 2022.
- [12] Leslie Rice, Anna Bair, Huan Zhang, and J Zico Kolter. Robustness between the worst and average case. *Advances in Neural Information Processing Systems*, 34:27840–27851, 2021.
- [13] Lily Weng, Pin-Yu Chen, Lam Nguyen, Mark Squillante, Akhilan Boopathy, Ivan Oseledets, and Luca Daniel. Proven: Verifying robustness of neural networks with a probabilistic approach. In *International Conference on Machine Learning*, pages 6727–6736. PMLR, 2019.
- [14] Roman Vershynin. *High-dimensional probability: An introduction with applications in data science*. Cambridge University Press, 2018.
- [15] Martin Pawelczyk, Teresa Datta, Johannes vanden Heuvel, Gjergji Kasneci, and Himabindu Lakkaraju. Probabilistically robust recourse: Navigating the trade-offs between costs and robustness in algorithmic recourse. *International Conference on Learning Representations*, 2023.
- [16] Zdravko I Botev. The normal law under linear restrictions: Simulation and estimation via minimax tilting. *Journal of the Royal Statistical Society. Series B (Statistical Methodology)*, 2017.
- [17] SciPy multivariate normal CDF. [https://docs.scipy.org/doc/scipy/reference/generated/scipy.stats.multivariate\\_normal.html](https://docs.scipy.org/doc/scipy/reference/generated/scipy.stats.multivariate_normal.html).
- [18] Billingsley Patrick. Probability and measure. *A Wiley-Interscience Publication, John Wiley*, 118: 119, 1995.
- [19] Suraj Srinivas, Kyle Matoba, Himabindu Lakkaraju, and François Fleuret. Efficient training of low-curvature neural networks. *Advances in Neural Information Processing Systems*, 35:25951–25964, 2022.
- [20] Tessa Han, Suraj Srinivas, and Himabindu Lakkaraju. Which explanation should I choose? A function approximation perspective to characterizing post hoc explanations. *Neural Information Processing Systems*, 2022.
- [21] Daniel Smilkov, Nikhil Thorat, Been Kim, Fernanda Viégas, and Martin Wattenberg. SmoothGrad: removing noise by adding noise. *arXiv preprint arXiv:1706.03825*, 2017.
- [22] Sushant Agarwal, Shahin Jabbari, Chirag Agarwal, Sohini Upadhyay, Steven Wu, and Himabindu Lakkaraju. Towards the unification and robustness of perturbation and gradient based explanations. *International Conference on Machine Learning*, 2021.

- [23] Dan Hendrycks and Kevin Gimpel. Gaussian error linear units (GELUs). *arXiv preprint arXiv:1606.08415*, 2016.
- [24] Li Deng. The MNIST database of handwritten digit images for machine learning research. *IEEE Signal Processing Magazine*, 2012.
- [25] Han Xiao, Kashif Rasul, and Roland Vollgraf. Fashion-MNIST: A novel image dataset for benchmarking machine learning algorithms. *arXiv preprint arXiv:1708.07747*, 2017.
- [26] Alex Krizhevsky, Geoffrey Hinton, et al. Learning multiple layers of features from tiny images. *University of Toronto*, 2009.
- [27] Kaiming He, Xiangyu Zhang, Shaoqing Ren, and Jian Sun. Deep residual learning for image recognition. *IEEE Conference on Computer Vision and Pattern Recognition*, 2016.
- [28] Francesco Croce, Maksym Andriushchenko, Vikash Sehwal, Edoardo DeBenedetti, Nicolas Flammarion, Mung Chiang, Prateek Mittal, and Matthias Hein. Robustbench: a standardized adversarial robustness benchmark. In *Thirty-fifth Conference on Neural Information Processing Systems Datasets and Benchmarks Track (Round 2)*, 2021.

## A Appendix

### A.1 Proofs

**Lemma A.1.** *The local robustness of a multi-class linear model  $f(\mathbf{x}) = \mathbf{w}^\top \mathbf{x} + b$  (with  $\mathbf{w} \in \mathbb{R}^{d \times C}$  and  $b \in \mathbb{R}^C$ ) at point  $\mathbf{x}$  with respect to a target class  $t$  is given by the following. Define weights  $\mathbf{u}_i = \mathbf{w}_t - \mathbf{w}_i \in \mathbb{R}^d, \forall i \neq t$ , where  $\mathbf{w}_t, \mathbf{w}_i$  are rows of  $\mathbf{w}$  and biases  $c_i = \mathbf{u}_i^\top \mathbf{x} + (b_t - b_i) \in \mathbb{R}$ . Then,*

$$p_\sigma^{\text{robust}}(\mathbf{x}) = \Phi_{\mathbf{U}\mathbf{U}^\top} \left( \frac{c_i}{\sigma \|\mathbf{u}_i\|_2} \Bigg|_{\substack{i=1 \\ i \neq t}}^C \right)$$

where  $\mathbf{U} = \frac{\mathbf{u}_i}{\|\mathbf{u}_i\|_2} \Bigg|_{\substack{i=1 \\ i \neq t}}^C \in \mathbb{R}^{(C-1) \times d}$

and  $\Phi_{\mathbf{U}\mathbf{U}^\top}$  is the  $(C-1)$ -dimensional Normal CDF with zero mean and covariance  $\mathbf{U}\mathbf{U}^\top$ .

*Proof.* First, we rewrite  $p_\sigma^{\text{robust}}$  in the following manner, by defining  $g_i(\mathbf{x}) = f_t(\mathbf{x}) - f_i(\mathbf{x}) > 0$ , which is the “decision boundary function”.

$$\begin{aligned} p_\sigma^{\text{robust}} &= P_{\epsilon \sim \mathcal{N}(0, \sigma^2)} \left[ \max_i f_i(\mathbf{x} + \epsilon) < f_t(\mathbf{x} + \epsilon) \right] \\ &= P_{\epsilon \sim \mathcal{N}(0, \sigma^2)} \left[ \bigcup_{i=1; i \neq t}^C g_i(\mathbf{x} + \epsilon) > 0 \right] \end{aligned}$$

Now, assuming that  $f, g$  are linear such that  $g_i(\mathbf{x}) = \mathbf{u}_i^\top \mathbf{x} + g(0)$ , we have  $g_i(\mathbf{x} + \epsilon) = g_i(\mathbf{x}) + \mathbf{u}_i^\top \epsilon$ , and obtain

$$\begin{aligned} p_\sigma^{\text{robust}} &= P_{\epsilon \sim \mathcal{N}(0, \sigma^2)} \left[ \bigcup_{i=1; i \neq t}^C \mathbf{u}_i^\top \epsilon > -g_i(\mathbf{x}) \right] \quad (1) \\ &= P_{z \sim \mathcal{N}(0, I_d)} \left[ \bigcup_{i=1; i \neq t}^C \frac{\mathbf{u}_i}{\|\mathbf{u}_i\|_2}^\top z > -\frac{g_i(\mathbf{x})}{\sigma \|\mathbf{u}_i\|_2} \right] \quad (2) \end{aligned}$$

This step simply involves rescaling and standardizing the Gaussian to be unit normal. We now make the following observations:

- For any matrix  $\mathbf{U} \in \mathbb{R}^{(C-1) \times d}$  and a  $d$ -dimensional Gaussian random variable  $z \sim \mathcal{N}(0, I_d) \in \mathbb{R}^d$ , we have  $\mathbf{U}^\top z \sim \mathcal{N}(0, \mathbf{U}\mathbf{U}^\top)$ , i.e., an  $(C-1)$ -dimensional Gaussian random variable.
- CDF of a multivariate Gaussian RV is defined as  $P_z[\bigcup_i z_i < t_i]$  for some input values  $t_i$

Using these observations, if we construct  $\mathbf{U} = \frac{\mathbf{u}_i}{\|\mathbf{u}_i\|_2} \Bigg|_{\substack{i=1 \\ i \neq t}}^C \in \mathbb{R}^{(C-1) \times d}$ , and obtain

$$\begin{aligned} p_\sigma^{\text{robust}} &= P_{r \sim \mathcal{N}(0, \mathbf{U}\mathbf{U}^\top)} \left[ \bigcup_{i=1; i \neq t}^C r_i < \frac{g_i(\mathbf{x})}{\sigma \|\mathbf{u}_i\|_2} \right] \\ &= \text{CDF}_{\mathcal{N}(0, \mathbf{U}\mathbf{U}^\top)} \left( \frac{g_i(\mathbf{x})}{\sigma \|\mathbf{u}_i\|_2} \Bigg|_{\substack{i=1 \\ i \neq t}}^C \right) \end{aligned}$$

where  $g_i(\mathbf{x}) = \mathbf{u}_i^\top \mathbf{x} + g_i(0) = (\mathbf{w}_t - \mathbf{w}_i)^\top \mathbf{x} + (b_t - b_i)$

□

**Lemma A.2. (Extension to non-Gaussian noise)** *For high-dimensional data ( $d \rightarrow \infty$ ), Lemma 1 generalizes to any coordinate-wise independent noise distribution that satisfies Lyapunov’s condition.*

*Proof.* Applying Lyapunov’s central limit theorem, given  $\epsilon \sim \mathcal{R}$  is sampled from some distribution  $\mathcal{R}$  to equation 2 in the previous proof, we have we have  $\frac{\mathbf{u}}{\sigma \|\mathbf{u}\|_2}^\top \epsilon = \sum_{j=1}^d \frac{\mathbf{u}_j}{\sigma \|\mathbf{u}\|_2} \epsilon_j \xrightarrow{d} \mathcal{N}(0, 1)$ , which holds as long as the sequence  $\{\frac{\mathbf{u}_j}{\|\mathbf{u}\|_2} \epsilon_j\}$  are independent random variables and satisfy the Lyapunov condition. In particular, this implies that  $\mathbf{U}^\top z \sim \mathcal{N}(0, \mathbf{U}\mathbf{U}^\top)$ , and the proof proceeds as similar to the Gaussian case after this step. □

**Lemma A.3. (Extension to non-isotropic Gaussian)** *Lemma 1 can be extended to the case of  $\epsilon \sim \mathcal{N}(0, \mathcal{C})$  for an arbitrary positive definite covariance matrix  $\mathcal{C}$ :*

$$p_\sigma^{\text{robust}}(\mathbf{x}) = \Phi_{\mathbf{U}\mathcal{C}\mathbf{U}^\top} \left( \frac{c_i}{\|\mathbf{u}_i\|_2} \Bigg|_{\substack{i=1 \\ i \neq t}}^C \right)$$

*Proof.* We observe that the Gaussian random variable  $\frac{\mathbf{u}_i}{\|\mathbf{u}_i\|_2}^\top \epsilon \Big|_{\substack{i=1 \\ i \neq t}}^C = \mathbf{U}^\top \epsilon$  has mean zero as  $\epsilon$  is mean zero. Computing its covariance matrix, we have  $\mathbb{E}_\epsilon \mathbf{U}^\top \epsilon \epsilon^\top \mathbf{U} = \mathbf{U}^\top \mathbb{E}_\epsilon (\epsilon \epsilon^\top) \mathbf{U} = \mathbf{U}^\top \mathcal{C} \mathbf{U}$ . We use this result after equation 2 in the proof of Lemma 1. □

**Proposition A.1.** *The Taylor estimator for the local robustness of a classifier  $f$  at point  $\mathbf{x}$  with respect to target class  $t$  is given by linearizing  $f$  around  $\mathbf{x}$  using a first-order Taylor expansion, with decision boundaries  $g_i(\mathbf{x}) = f_t(\mathbf{x}) - f_i(\mathbf{x})$ ,  $\forall i \neq t$ , leading to*

$$p_\sigma^{taylor}(\mathbf{x}) = \Phi_{\mathbf{U}\mathbf{U}^\top} \left( \frac{g_i(\mathbf{x})}{\sigma \|\nabla_{\mathbf{x}} g_i(\mathbf{x})\|_2} \Big|_{\substack{i=1 \\ i \neq t}}^C \right)$$

with  $\mathbf{U}$  and  $\Phi$  defined as in the linear case.

*Proof.* Using the notations from the previous Lemma A.1, we can linearize  $g(\mathbf{x} + \epsilon) \approx g(\mathbf{x}) + \nabla_{\mathbf{x}} g(\mathbf{x})^\top \epsilon$  using a first order Taylor series expansion. Thus we use  $\mathbf{u}_i = \nabla_{\mathbf{x}} g_i(\mathbf{x})$  and  $c_i = g_i(\mathbf{x})$ , and plug it into the result of Lemma A.1.  $\square$

**Proposition A.2.** *The estimation error of the Taylor estimator for a classifier with a quadratic decision boundary  $g_i(\mathbf{x}) = \mathbf{x}^\top A_i \mathbf{x} + \mathbf{u}_i^\top \mathbf{x} + c_i$  for positive-definite  $A_i$ , is upper bounded by*

$$|p_\sigma^{robust}(\mathbf{x}) - p_\sigma^{taylor}(\mathbf{x})| \leq k \sigma^{C-1} \prod_{\substack{i=1 \\ i \neq t}}^C \frac{\lambda_{\max}^{A_i}}{\|\mathbf{u}_i\|_2}$$

for noise  $\epsilon \sim \mathcal{N}(0, \sigma^2/d)$ , in the limit of  $d \rightarrow \infty$ .

*Proof.* Without loss of generality, assume that  $\mathbf{x} = 0$ . For any other  $\mathbf{x}_1 \neq 0$ , we can simply perform a change of variables of the underlying function to center it at  $\mathbf{x}_1$  to yield a different quadratic. We first write an expression for  $p_\sigma^{robust}$  for the given quadratic classifier  $g_i(\mathbf{x})$  at  $\mathbf{x} = 0$ .

$$\begin{aligned} p_\sigma^{robust}(0) &= P_\epsilon \left( \bigcup_i g_i(\epsilon) > 0 \right) \\ &= P_\epsilon \left( \bigcup_i \mathbf{u}_i^\top \epsilon + c > -\epsilon^\top A_i \epsilon \right) \end{aligned}$$

Similarly, computing,  $p_\sigma^{taylor}$  we have  $\nabla_{\mathbf{x}} g_i(0) = \mathbf{u}^\top$  and  $g_i(0) = c_i$ , resulting in

$$\begin{aligned} p_\sigma^{taylor}(0) &= P_\epsilon \left( \bigcup_i g_i^{taylor}(\epsilon) > 0 \right) \\ &= P_\epsilon \left( \bigcup_i \mathbf{u}_i^\top \epsilon + c > 0 \right) \end{aligned}$$

Subtracting the two, we have

$$\begin{aligned} &|p_\sigma^{robust}(0) - p_\sigma^{taylor}(0)| \\ &= \left| P \left( \bigcup_i 0 > \mathbf{u}_i^\top \epsilon + c > -\epsilon^\top A_i \epsilon \right) \right| \\ &= \left| P \left( \bigcup_i 0 > \frac{\mathbf{u}_i^\top \epsilon + c}{\sigma \|\mathbf{u}_i\|_2} > -\frac{\epsilon^\top A_i \epsilon}{\sigma \|\mathbf{u}_i\|_2} \right) \right| \end{aligned}$$

For high-dimensional Gaussian noise  $\epsilon \sim \mathcal{N}(0, \sigma^2/d)$ , with  $d \rightarrow \infty$ , we have that  $\|\epsilon\|^2 = \sum_i \epsilon_i^2 \rightarrow \sigma^2$  from the law of large numbers. See (14) for an extended discussion. Thus we have  $\epsilon^\top A_i \epsilon \leq \lambda_{\max}^A \|\epsilon\|^2 = \lambda_{\max}^A \sigma^2$ .

Also let  $z_i = \frac{\mathbf{u}_i^\top \epsilon + c}{\sigma \|\mathbf{u}_i\|_2}$  be a random variable. We observe that  $z_i|_i$  is a tensor extension of  $z_i$ , has a covariance matrix of  $\mathbf{U}\mathbf{U}^\top$  as before. Let us also define  $C_i = \frac{\lambda_{\max}^{A_i}}{\|\mathbf{u}_i\|_2}$ .

$$\begin{aligned} &|p_\sigma^{robust}(0) - p_\sigma^{taylor}(0)| \\ &= \left| P \left( \bigcup_i 0 > z_i(\epsilon) > -\frac{\epsilon^\top A_i \epsilon}{\sigma \|\mathbf{u}_i\|_2} \right) \right| \\ &\leq \left| P \left( \bigcup_i 0 > z_i > -\frac{\lambda_{\max}^{A_i}}{\|\mathbf{u}_i\|_2} \sigma \right) \right| \quad (\epsilon^\top A_i \epsilon < \lambda_{\max}^A \sigma^2) \\ &= \left| \int \dots \int_{-C_i \sigma}^0 \text{pdf}(z_i|_i) dz_i|_i \right| \quad (\text{Defn of mvn cdf}) \\ &\leq \max_{z_i|_i} \text{pdf}(z_i|_i) \prod_i |C_i \sigma| \quad (\text{Upper bound pdf with its max}) \\ &\leq (2\pi)^{-(C-1)/2} \det(\mathbf{U}\mathbf{U}^\top)^{-1/2} \prod_{\substack{i=1 \\ i \neq t}}^C C_i \sigma \\ &= k \left( \sigma^{C-1} \prod_{\substack{i=1 \\ i \neq t}}^C \frac{\lambda_{\max}^{A_i}}{\|\mathbf{u}_i\|_2} \right) \end{aligned}$$

where  $k = \max_z \text{pdf}(z) = (2\pi)^{-(C-1)/2} \det(\mathbf{U}\mathbf{U}^\top)^{-1/2}$ , which is the max value of the Gaussian pdf. Note that as the rows of  $\mathbf{U}$  are normalized,  $\det(\mathbf{U}) \leq 1$  and  $\det(\mathbf{U}\mathbf{U}^\top) = \det(\mathbf{U})^2 \leq 1$ .  $\square$

We note that these bounds are rather pessimistic, as in high-dimensions  $\epsilon^\top A_i \epsilon \sim \lambda_{\text{mean}}^{A_i} \leq \lambda_{\max}^{A_i}$ , and thus in reality the errors are expected to be much smaller.

**Proposition A.3.** *The MMSE estimator for the local robustness of a classifier  $f$  at point  $\mathbf{x}$  with respect to target class  $t$  is given by an MMSE linearization  $f$*

around  $\mathbf{x}$ , for decision boundaries  $g_i(\mathbf{x}) = f_t(\mathbf{x}) - f_i(\mathbf{x})$ ,  $\forall i \neq t$ , leading to

$$p_\sigma^{mmse}(\mathbf{x}) = \Phi_{\mathbf{U}\mathbf{U}^\top} \left( \frac{\tilde{g}_i(\mathbf{x})}{\sigma \|\nabla_{\mathbf{x}} \tilde{g}_i(\mathbf{x})\|_2} \Big|_{\substack{i=1 \\ i \neq t}}^C \right)$$

where  $\tilde{g}_i(\mathbf{x}) = \frac{1}{N} \sum_{j=1}^N g_i(\mathbf{x} + \epsilon)$ ,  $\epsilon \sim \mathcal{N}(0, \sigma^2)$

with  $\mathbf{U}$  and  $\Phi$  defined as in the linear case, and  $N$  is the number of perturbations.

*Proof.* We would like to improve upon the Taylor approximation to  $g(\mathbf{x} + \epsilon)$  by using an MMSE local function approximation. Essentially, we'd like to find  $\mathbf{u} \in \mathbb{R}^d$  and  $c \in \mathbb{R}$  such that

$$(\mathbf{u}^*(\mathbf{x}), c^*(\mathbf{x})) = \arg \min_{\mathbf{u}, c} \mathbb{E}_{\epsilon \sim \mathcal{N}(0, \sigma^2)} (g(\mathbf{x} + \epsilon) - \mathbf{u}^\top \epsilon - c)^2$$

A straightforward solution by finding critical points and equating it to zero gives us the following:

$$\begin{aligned} \mathbf{u}^*(\mathbf{x}) &= \mathbb{E}_\epsilon [g(\mathbf{x} + \epsilon) \epsilon^\top] / \sigma^2 \\ &= \mathbb{E}_\epsilon [\nabla_{\mathbf{x}} g(\mathbf{x} + \epsilon)] \quad (\text{Stein's Lemma}) \\ c^*(\mathbf{x}) &= \mathbb{E}_\epsilon g(\mathbf{x} + \epsilon) \end{aligned}$$

Plugging in these values of  $\mathbf{u}^*$ ,  $c^*$  into Lemma A.1, we have the result.  $\square$

**Proposition A.4.** *The estimation error of the MMSE estimator for a classifier with a quadratic decision boundary  $g(\mathbf{x}) = \mathbf{x}^\top \mathbf{A} \mathbf{x} + \mathbf{u}^\top \mathbf{x} + c$ , and positive definite  $\mathbf{A}$  is upper bounded by*

$$|p_\sigma^{robust}(\mathbf{x}) - p_\sigma^{mmse}(\mathbf{x})| \leq k \sigma^{C-1} \prod_{\substack{i=1 \\ i \neq t}}^C \frac{|\lambda_{\max}^{A_i} - \lambda_{\text{mean}}^{A_i}|}{\|\mathbf{u}_i\|_2}$$

for noise  $\epsilon \sim \mathcal{N}(0, \sigma^2/d)$ , in the limit of  $d \rightarrow \infty$  and  $N \rightarrow \infty$ .

*Proof.* We proceed similarly to the proof made for the Taylor estimator, and without loss of generality, assume that  $\mathbf{x} = 0$ . Computing,  $p_\sigma^{mmse}$  we have  $\mathbb{E}_\epsilon \nabla_{\mathbf{x}} g_i(\epsilon) = \mathbf{u}_i^\top$  and  $\mathbb{E}_\epsilon g_i(\epsilon) = c + \mathbb{E}(\epsilon^\top A_i \epsilon) =$

$c + \mathbb{E}(\text{trace}(\epsilon^\top A_i \epsilon)) = c + \mathbb{E}(\text{trace}(A_i \epsilon \epsilon^\top)) = c + \text{trace}(A_i) \sigma^2/d = c + \sigma^2 \lambda_{\text{mean}}^{A_i}$ , resulting in

$$\begin{aligned} p_\sigma^{mmse}(0) &= P_\epsilon \left( \bigcup_i \hat{g}_i(\epsilon) > 0 \right) \\ &= P_\epsilon \left( \bigcup_i \mathbf{u}_i^\top \epsilon + c > -\sigma^2 \lambda_{\text{mean}}^{A_i} \right) \end{aligned}$$

Subtracting the two, we have

$$\begin{aligned} &|p_\sigma^{robust}(0) - p_\sigma^{mmse}(0)| \\ &\leq \left| P \left( \bigcup_i -\sigma^2 \lambda_{\text{mean}}^{A_i} > \mathbf{u}_i^\top \epsilon + c > -\sigma^2 \lambda_{\max}^{A_i} \right) \right| \\ &= \left| P \left( \bigcup_i -\sigma \frac{\lambda_{\text{mean}}^{A_i}}{\|\mathbf{u}_i\|_2} > \frac{\mathbf{u}_i^\top \epsilon + c}{\sigma \|\mathbf{u}_i\|_2} > -\sigma \frac{\lambda_{\max}^{A_i}}{\|\mathbf{u}_i\|_2} \right) \right| \end{aligned}$$

Similar to the previous proof, let  $z_i = \mathbf{u}_i^\top \epsilon + c$  be a random variable, and that  $z_i | i$  is a tensor extension of  $z_i$  from our previous notation.

$$\begin{aligned} &|p_\sigma^{robust}(\mathbf{x}) - p_\sigma^{mmse}(\mathbf{x})| \\ &\leq \left| P \left( \bigcup_i -\lambda_{\text{mean}}^{A_i} \sigma^2 > z_i > -\lambda_{\max}^{A_i} \sigma^2 \right) \right| \\ &= \left| \int \dots \int_{-\lambda_{\max}^{A_i} \sigma^2}^{-\lambda_{\text{mean}}^{A_i} \sigma^2} \text{pdf}(z_i | i) dz_i | i \right| \\ &\leq \max_{z_i | i} \text{pdf}(z_i | i) \sigma^{C-1} \prod_i \frac{|\lambda_{\max}^{A_i} - \lambda_{\text{mean}}^{A_i}|}{\|\mathbf{u}_i\|_2} \\ &= k \sigma^{C-1} \prod_i \frac{|\lambda_{\max}^{A_i} - \lambda_{\text{mean}}^{A_i}|}{\|\mathbf{u}_i\|_2} \end{aligned}$$

where  $k = \max_z \text{pdf}(z_i | i) = (2\pi)^{-(C-1)/2} \det(\mathbf{U}\mathbf{U}^\top)^{-1/2}$  like in the Taylor case. Note that as the rows of  $\mathbf{U}$  are normalized,  $\det(\mathbf{U}) \leq 1$  and  $\det(\mathbf{U}\mathbf{U}^\top) = \det(\mathbf{U})^2 \leq 1$ .  $\square$

We note that these bounds are rather pessimistic, as in high-dimensions  $\epsilon^\top A_i \epsilon \sim \lambda_{\text{mean}}^{A_i} \leq \lambda_{\max}^{A_i}$ , and thus in reality the errors are expected to be much smaller.

**The softmax estimator** We observe that for linear models with a specific noise perturbation  $\sigma$ , the common softmax function taken with respect to the output

logits can be viewed as an estimator of  $p_\sigma^{\text{robust}}$ , albeit in a very restricted setting. Specifically,

**Lemma A.4.** *For multi-class linear models  $f(\mathbf{x}) = \mathbf{w}^\top \mathbf{x} + b$ , such that the decision boundary weight norms  $\|\mathbf{u}_i\|_2 = k, \forall i \in [1, C], i \neq t$ ,*

$$p_T^{\text{softmax}} = p_\sigma^{\text{taylor\_mvs}} \quad \text{where} \quad T = \sigma k$$

*Proof.* Consider softmax with respect to the  $t^{\text{th}}$  output class and define  $g_i(\mathbf{x}) = f_t(\mathbf{x}) - f_i(\mathbf{x})$ , with  $f$  being the linear model logits. Using this, we first show that softmax is identical to *mv-sigmoid*:

$$\begin{aligned} p_T^{\text{softmax}}(\mathbf{x}) &= \text{softmax}_t(f_1(\mathbf{x})/T, \dots, f_C(\mathbf{x})/T) \\ &= \frac{\exp(f_t(\mathbf{x})/T)}{\sum_i \exp(f_i(\mathbf{x})/T)} \\ &= \frac{1}{1 + \sum_{i:i \neq t} \exp((f_i(\mathbf{x}) - f_t(\mathbf{x}))/T)} \\ &= \text{mv-sigmoid} \left[ g_i(\mathbf{x})/T \left| \begin{array}{c} C \\ i=1 \\ i \neq t \end{array} \right. \right] \end{aligned}$$

Next, by denoting  $\mathbf{u}_i = \mathbf{w}_t - \mathbf{w}_i$ , each row has equal norm  $\|\mathbf{u}_i\|_2 = \|\mathbf{u}_j\|_2, \forall i, j, t \in [1, \dots, C]$  which implies:

$$\begin{aligned} p_\sigma^{\text{taylor\_mvs}}(\mathbf{x}) &= \text{mv-sigmoid} \left[ \frac{g_i(\mathbf{x})}{\sigma \|\mathbf{u}_i\|_2} \left| \begin{array}{c} C \\ i=1 \\ i \neq t \end{array} \right. \right] \\ &= \text{mv-sigmoid} \left[ g_i(\mathbf{x})/T \left| \begin{array}{c} C \\ i=1 \\ i \neq t \end{array} \right. \right] \quad (\because T = \sigma k) \\ &= p_T^{\text{softmax}}(\mathbf{x}) \end{aligned}$$

□

Lemma A.4 indicates that the temperature parameter  $T$  of softmax roughly corresponds to the  $\sigma$  of the added Normal noise with respect to which local robustness is measured. Overall, this shows that under the restricted setting where the local linear model consists of decision boundaries with equal weight norms, the softmax outputs can be viewed as an estimator of the  $p_\sigma^{\text{taylor\_mvs}}$  estimator, which itself is an estimator of  $p_\sigma^{\text{robust}}$ . However, due to the multiple levels of approximation, we can expect the quality of  $p_T^{\text{softmax}}$ 's approximation of  $p_\sigma^{\text{robust}}$  to be poor in general settings (outside of the very restricted setting), so much so that in general settings,  $p_\sigma^{\text{robust}}$  and  $p_T^{\text{softmax}}$  would be unrelated.

## A.2 Datasets

The MNIST dataset consists of images of gray-scale handwritten digits spanning 10 classes: digits 0 through 9. The FashionMNIST (FMNIST) dataset consists of gray-scale images of articles of clothing spanning 10 classes: t-shirt, trousers, pullover, dress, coat, sandal, shirt, sneaker, bag, and ankle boot. For MNIST and FMNIST, each image is 28 pixels x 28 pixels. For MNIST and FMNIST, the training set consists of 60,000 images and the test set consists of 10,000 images.

The CIFAR10 dataset consists of color images of common objects and animals spanning 10 classes: airplane, car, bird, cat, deer, dog, frog, horse, ship, and truck. The CIFAR100 dataset consists of color images of common objects and animals spanning 100 classes: apple, bowl, chair, dolphin, lamp, mouse, plain, rose, squirrel, train, etc. For CIFAR10 and CIFAR100, each image is 3 pixels x 32 pixels x 32 pixels. For CIFAR10 and CIFAR100, the training set consists of 50,000 images and the test set consists of 10,000 images.

## A.3 Models

For the MNIST and FMNIST, we train a linear model and a convolutional neural network (CNN) to perform 10-class classification. The linear model consists of one hidden layer with 10 neurons. The CNN consists of four hidden layers: one convolutional layer with 5x5 filters and 10 output channels, one convolutional layer 5x5 filters and 20 output channels, and one linear layer with 50 neurons, and one linear layer 10 neurons.

For CIFAR10 and CIFAR100, we train a ResNet18 model to perform 10-class and 100-class classification, respectively. The model architecture is described in (27). We train the ResNet18 models using varying levels of gradient norm regularization to obtain models with varying levels of robustness. The larger the weight of gradient norm regularization ( $\lambda$ ), the more robust the model.

All models were trained using stochastic gradient descent. Hyperparameters were selected to achieve decent model performance. The emphasis is on analyzing the estimators' estimates of local robustness of each model, not on high model performance. Thus, we do not focus on tuning model hyperparameters. All models were trained for 200 epochs. The test set accuracy for each model is shown in Table 2.

## A.4 Experiments

In this section, we provide the following additional experimental results:

Dataset	Model	$\lambda$	Test set accuracy
MNIST	Linear	0	92%
MNIST	CNN	0	99%
FashionMNIST	Linear	0	84%
FashionMNIST	CNN	0	91%
CIFAR10	ResNet18	0	94%
CIFAR10	ResNet18	0.0001	93%
CIFAR10	ResNet18	0.001	90%
CIFAR10	ResNet18	0.01	85%
CIFAR100	ResNet18	0	76%
CIFAR100	ResNet18	0.0001	74%
CIFAR100	ResNet18	0.001	69%
CIFAR100	ResNet18	0.01	60%

Table 2: Test set accuracy of models.

- Figure 5 shows results on the convergence of  $p_\sigma^{\text{mc}}$ .  $p_\sigma^{\text{mc}}$  takes a large number of samples to converge and is computationally inefficient.
- Figure 6 shows results on the convergence of  $p_\sigma^{\text{mmse}}$ .  $p_\sigma^{\text{mmse}}$  takes only a few samples to converge and is more computationally inefficient than  $p_\sigma^{\text{mc}}$ .
- Figure 7 shows the distribution of  $p_\sigma^{\text{robust}}$  as a function of  $\sigma$ . Consistent with theory in Section 3, (1) as noise increases,  $p_\sigma^{\text{robust}}$  decreases, and (2)  $p_\sigma^{\text{mmse}}$  accurately estimates  $p_\sigma^{\text{mc}}$ .
- Table 3 presents estimator runtimes. Our analytical estimators are more efficient than the naïve estimator ( $p_\sigma^{\text{mc}}$ ).
- Figure 8 shows the accuracy of the analytical robustness estimators as a function of  $\sigma$ .  $p_\sigma^{\text{mmse}}$  and  $p_{\sigma}^{\text{mmse}-\text{mvs}}$  are the best estimators of  $p_\sigma^{\text{robust}}$ , followed closely by  $p_{\sigma}^{\text{taylor}-\text{mvs}}$  and  $p_{\sigma}^{\text{taylor}}$ , trailed by  $p_T^{\text{softmax}}$ .
- Figure 9 shows the accuracy of the analytical estimators for robust models. For more robust models, the estimators compute  $p_\sigma^{\text{robust}}$  more accurately over a larger  $\sigma$ .
- Figure 10 shows that *mv-sigmoid* well-approximates *mvn-cdf* over  $\sigma$ .
- Figure 11 shows the distribution of  $p_\sigma^{\text{robust}}$  among classes (measured by  $p_\sigma^{\text{mmse}}$ ), revealing that models display robustness bias among classes.
- Figures 12 and 13 show the application of  $p_\sigma^{\text{mmse}}$  and  $p_T^{\text{softmax}}$  to identification of robust and non-robust points.  $p_\sigma^{\text{robust}}$  better identifies robust and non-robust points than  $p_T^{\text{softmax}}$ .

- Figures 14, 15, 16, and 17 show examples of noisy images with the level of noise analyzed in our paper. Overall, the noise levels seem visually significant.

#### A.4.1 $p_\sigma^{\text{robust}}$ identifies images that are robust to and images that are vulnerable to random noise

For each dataset, we train a simple CNN to distinguish between images with high and low  $p_\sigma^{\text{mmse}}$ . We train the same CNN to also distinguish between images with high and low  $p_T^{\text{softmax}}$ . The CNN consists of two convolutional layers and two fully-connected feedforward layers with a total of 21,878 parameters. For a given dataset, for each class, we take the images with the top-25 and bottom-25  $p_\sigma^{\text{mmse}}$  values. This yields 500 images for CIFAR10 (10 classes x 50 images per class) and 5,000 images for CIFAR100 (100 classes x 50 images per class). We also perform the same steps using  $p_T^{\text{softmax}}$ , yielding another 500 images for CIFAR10 and another 5,000 images for CIFAR100. For each dataset, the train/test split is 90%/10% of points.

Then, we compare the performance of the two models. For CIFAR10, the test set accuracy for the  $p_\sigma^{\text{mmse}}$  CNN is 0.92 while that for the  $p_T^{\text{softmax}}$  CNN is 0.58. For CIFAR100, the test set accuracy for the  $p_\sigma^{\text{mmse}}$  CNN is 0.74 while that for the  $p_T^{\text{softmax}}$  CNN is 0.55. The higher the test set accuracy of a CNN, the better the CNN distinguishes between images. Thus, the results indicate that  $p_\sigma^{\text{robust}}$  better identifies images that are robust to and vulnerable to random noise than  $p_T^{\text{softmax}}$ .

We also provide additional visualizations of images with the highest and lowest  $p_\sigma^{\text{robust}}$  and images with the highest and lowest  $p_T^{\text{softmax}}$ .

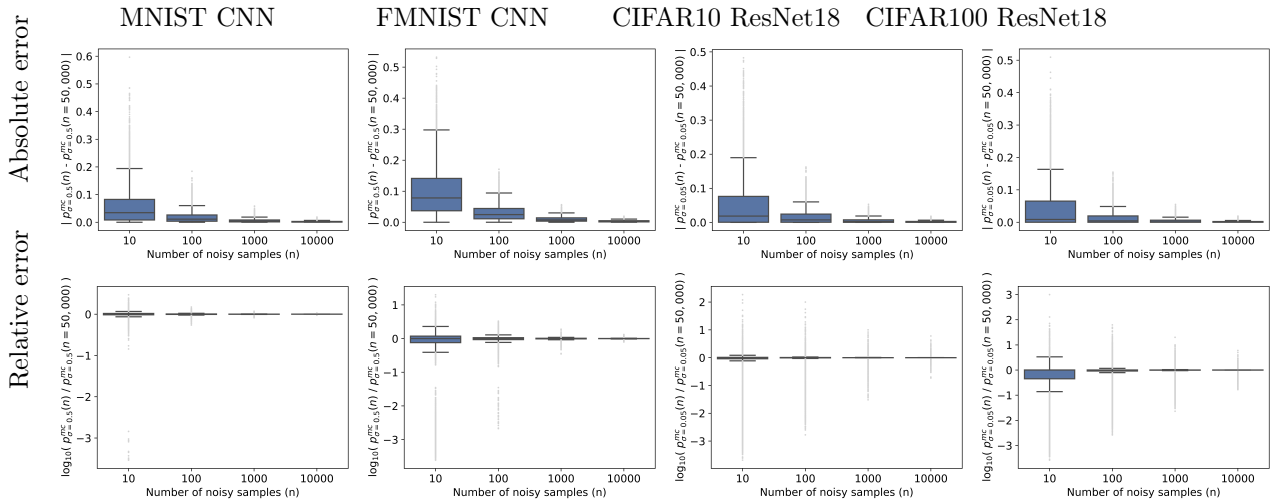


Figure 5: Convergence of  $p_{\sigma}^{mc}$ . In practice,  $p_{\sigma}^{mc}$  takes around  $n = 10,000$  samples to converge and is computationally inefficient.

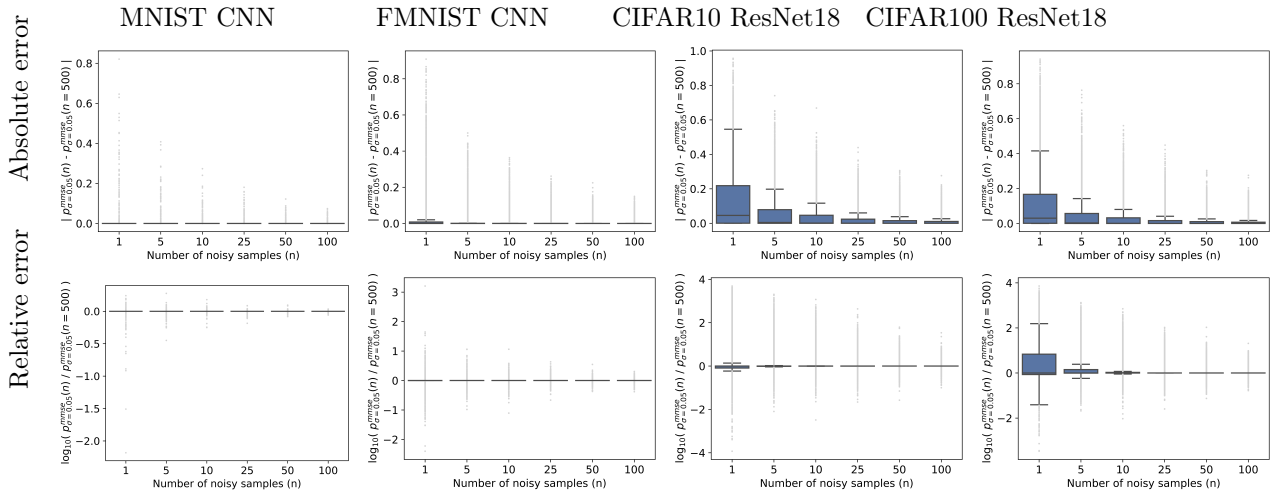


Figure 6: Convergence of  $p_{\sigma}^{mmse}$ . In practice,  $p_{\sigma}^{mmse}$  takes around  $n = 5 - 10$  samples to converge and is more computationally inefficient than  $p_{\sigma}^{mc}$ .

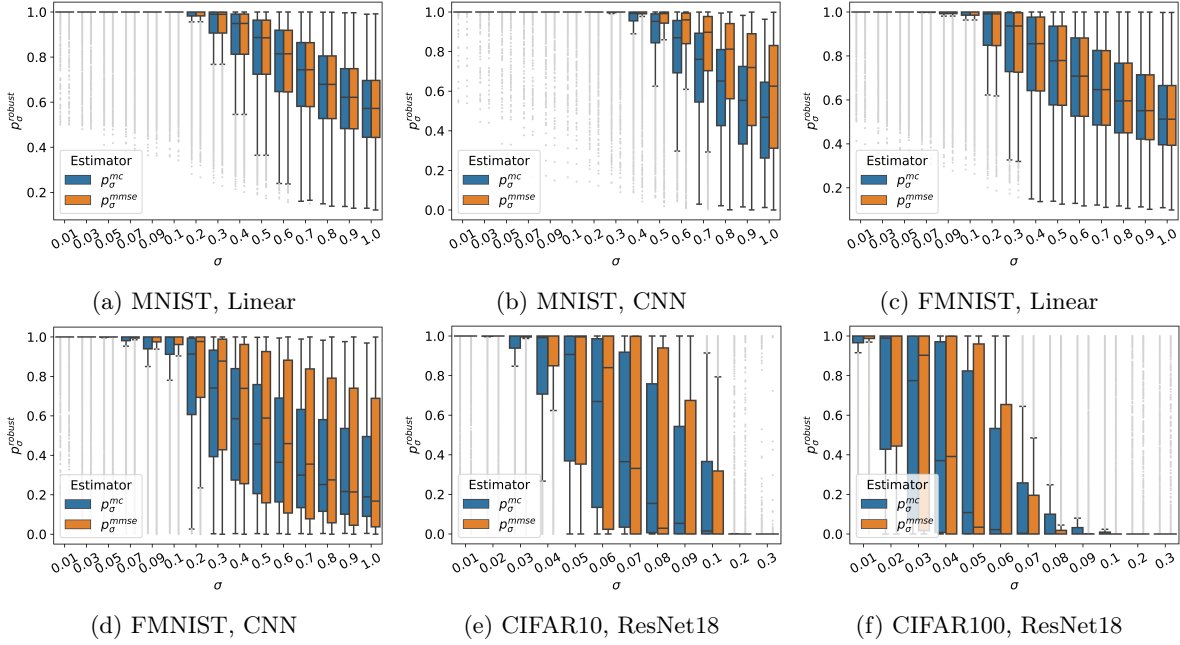


Figure 7: Distribution of  $p_\sigma^{\text{robust}}$  over  $\sigma$ . As noise increases,  $p_\sigma^{\text{robust}}$  decreases. In addition,  $p_\sigma^{\text{mmse}}$  accurately estimates  $p_\sigma^{\text{mc}}$ .

		CPU: Intel x86_64		GPU: Tesla V100-PCIE-32GB	
Estimator	# samples ( $n$ )	Serial	Batched	Serial	Batched
$p_\sigma^{\text{mc}}$	<i><math>n = 100</math></i>	0:00:59	0:00:42	0:00:12	0:00:01
	<i><math>n = 1000</math></i>	0:09:50	0:07:22	0:02:00	0:00:04
	<i><math>n = 10000</math></i>	1:41:11	1:14:38	0:19:56	0:00:35
$p_\sigma^{\text{taylor}}$	N/A	0:00:08	0:00:07	0:00:02	< 0:00:01
$p_\sigma^{\text{taylor\_mvs}}$	N/A	0:00:08	0:00:07	0:00:01	< 0:00:01
$p_\sigma^{\text{mmse}}$	<i><math>n = 1</math></i>	0:00:08	0:00:10	0:00:02	0:00:02
	<i><math>n = 5</math></i>	0:00:41	0:00:31	0:00:06	0:00:02
	<i><math>n = 10</math></i>	0:01:21	0:01:02	0:00:11	0:00:02
	<i><math>n = 25</math></i>	0:03:21	0:02:44	0:00:26	0:00:03
	<i><math>n = 50</math></i>	0:06:47	0:05:38	0:00:51	0:00:04
	<i><math>n = 100</math></i>	0:13:57	0:11:31	0:01:42	0:00:06
$p_\sigma^{\text{mmse\_mvs}}$	<i><math>n = 1</math></i>	0:00:08	0:00:08	0:00:01	0:00:01
	<i><math>n = 5</math></i>	0:00:41	0:00:32	0:00:05	0:00:01
	<i><math>n = 10</math></i>	0:01:21	0:01:00	0:00:10	0:00:02
	<i><math>n = 25</math></i>	0:03:24	0:02:37	0:00:25	0:00:02
	<i><math>n = 50</math></i>	0:06:47	0:05:35	0:00:51	0:00:03
	<i><math>n = 100</math></i>	0:13:28	0:11:32	0:01:42	0:00:06
$p_T^{\text{softmax}}$	N/A	0:00:01	< 0:00:01	< 0:00:01	< 0:00:01

Table 3: Runtimes of each  $p_\sigma^{\text{robust}}$  estimator. Each estimator computes  $p_{\sigma=0.1}^{\text{robust}}$  for the CIFAR10 ResNet18 model for 50 data points. For estimators that use sampling, the row with the minimum number of samples necessary for convergence is italicized. Runtimes are in the format of hour:minute:second. The analytical estimators ( $p_\sigma^{\text{taylor}}$ ,  $p_\sigma^{\text{taylor\_mvs}}$ ,  $p_\sigma^{\text{mmse}}$ , and  $p_\sigma^{\text{mmse\_mvs}}$ ) are more efficient than the naïve estimator ( $p_\sigma^{\text{mc}}$ ).

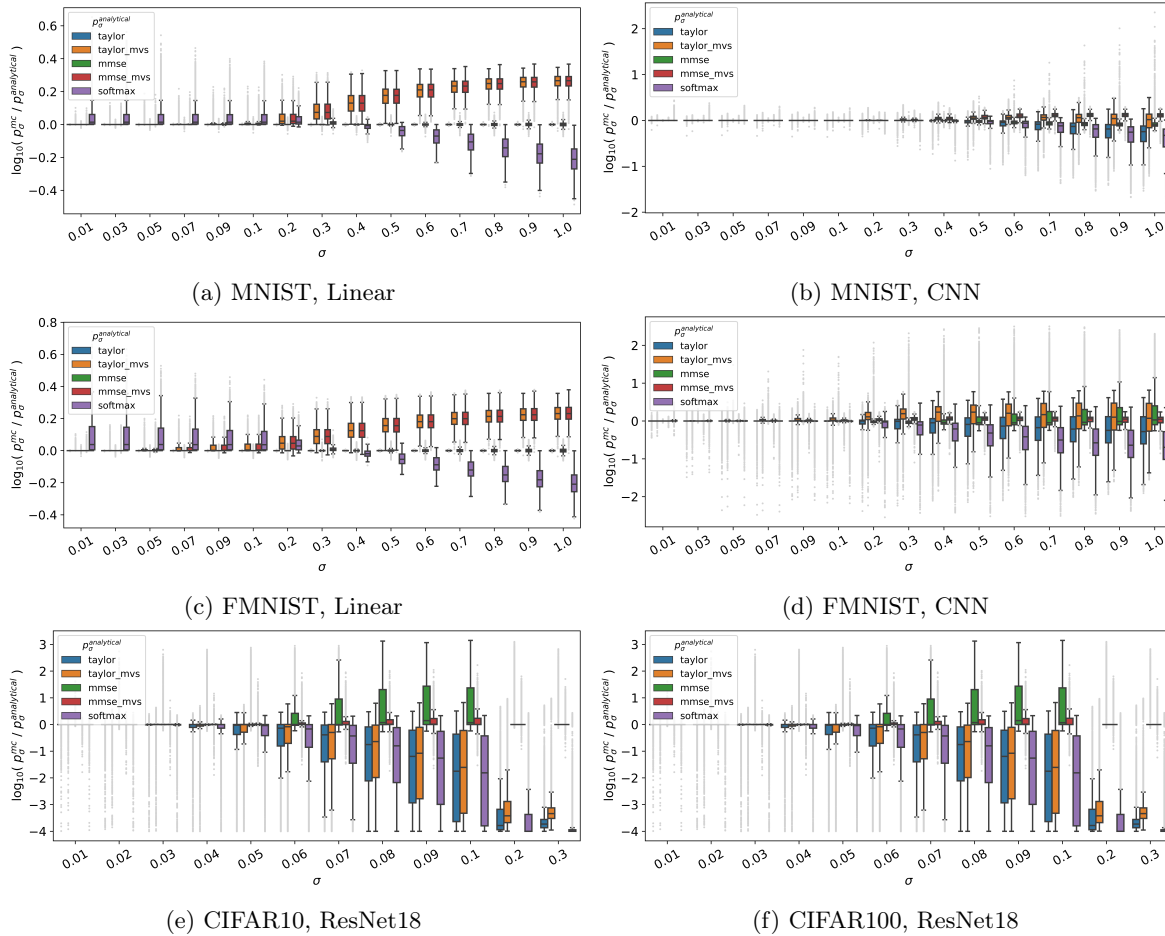


Figure 8: Accuracy of  $p_\sigma^{\text{robust}}$  estimators over  $\sigma$ . The smaller the noise neighborhood  $\sigma$ , the more accurately the estimators compute  $p_\sigma^{\text{robust}}$ .  $p_\sigma^{\text{mmse}}$  and  $p_\sigma^{\text{mmse\_mvms}}$  are the best estimators of  $p_\sigma^{\text{robust}}$ , followed closely by  $p_\sigma^{\text{taylor\_mvms}}$  and  $p_\sigma^{\text{taylor}}$ , trailed by  $p_\sigma^{\text{softmax}}$ .

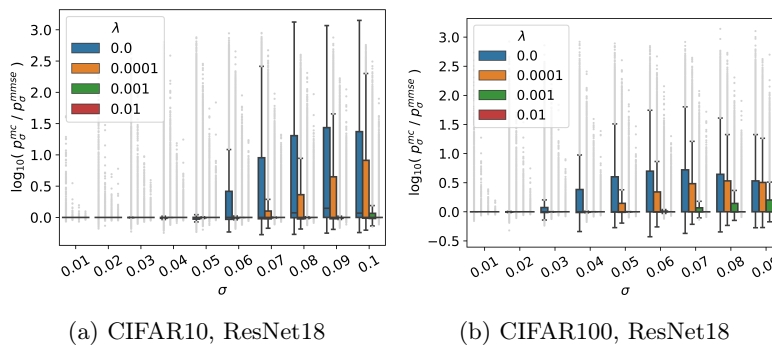


Figure 9: Accuracy of  $p_\sigma^{\text{robust}}$  estimators over  $\sigma$  for robust models. For more robust models, the estimators compute  $p_\sigma^{\text{robust}}$  more accurately over a larger  $\sigma$ .

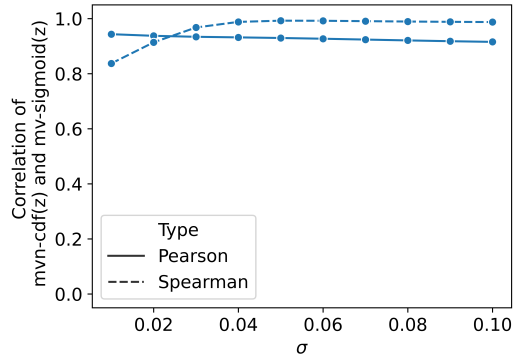


Figure 10: mv-sigmoid’s approximation of mvn-cdf over  $\sigma$ . mv-sigmoid well-approximates mvn-cdf over  $\sigma$ .

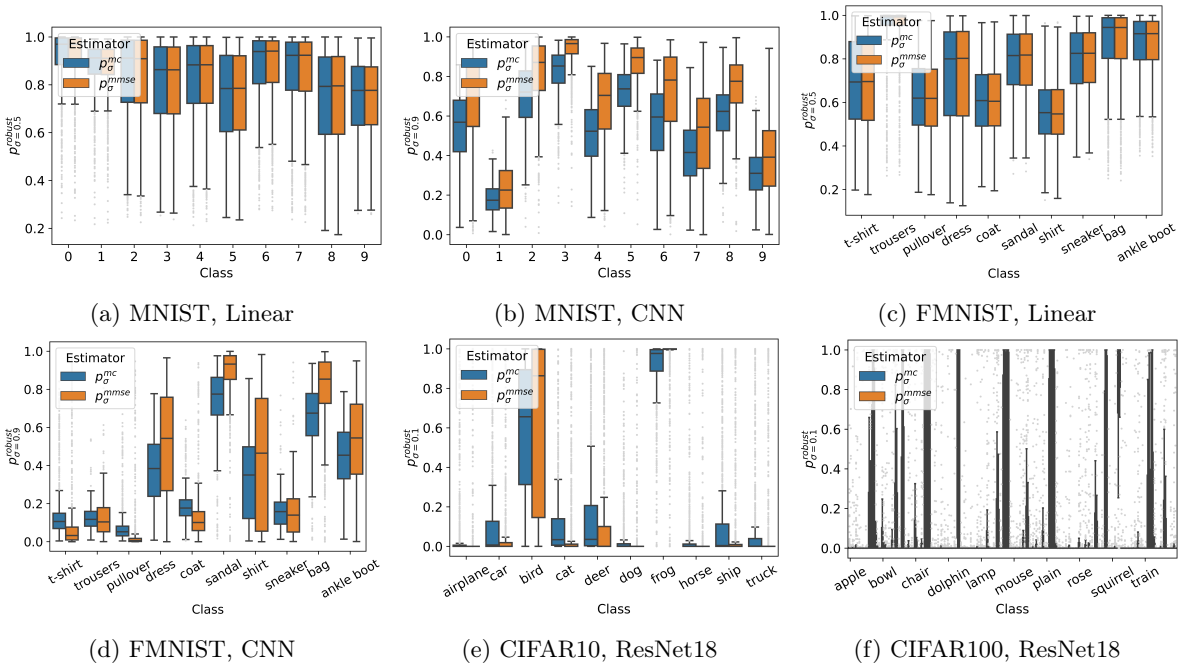


Figure 11: Local robustness bias among classes.  $p_{\sigma}^{\text{robust}}$  reveals that the model is less locally robust for some classes than for others. The analytical estimator  $p_{\sigma}^{\text{mmse}}$  properly captures this model bias.

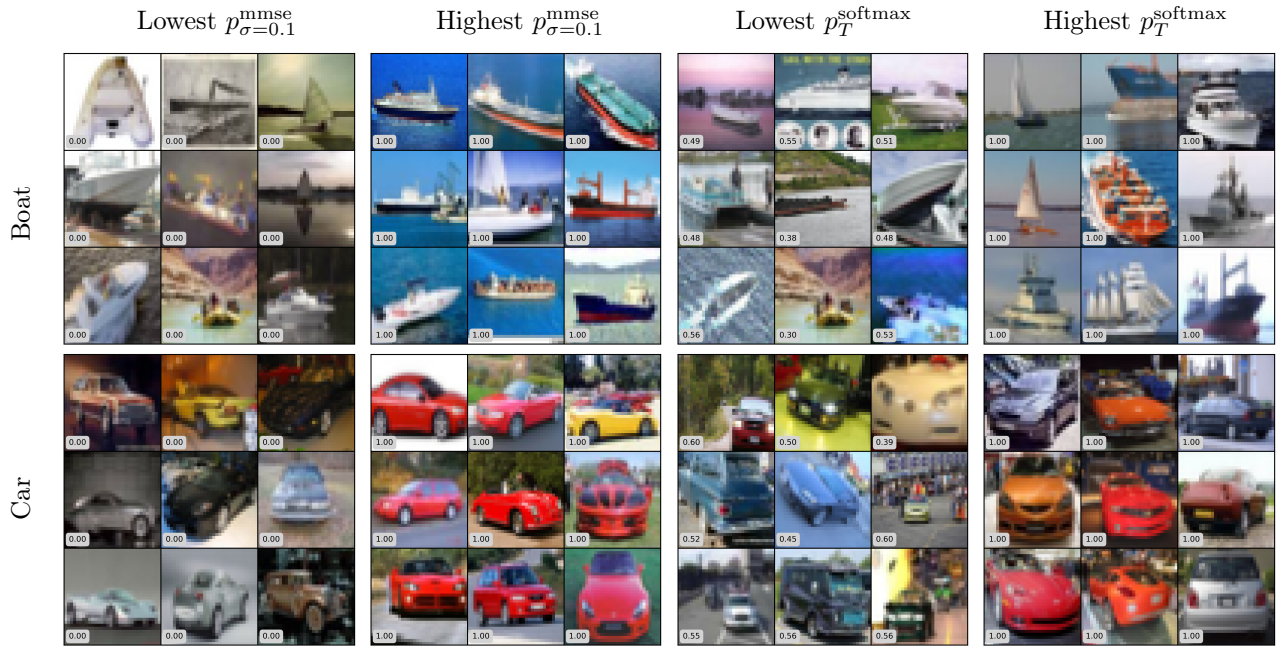


Figure 12: Additional images with the lowest and highest  $p_{\sigma}^{\text{robust}}$  and  $p_T^{\text{softmax}}$  values among CIFAR10 classes. Images with high  $p_{\sigma}^{\text{robust}}$  tend to be brighter and have stronger object-background contrast (making them more robust to random noise) than those with low  $p_{\sigma}^{\text{robust}}$ . The difference between images with high and low  $p_T^{\text{softmax}}$  is less clear. Thus,  $p_{\sigma}^{\text{robust}}$  better captures the model’s local robustness with respect to an input than  $p_T^{\text{softmax}}$ .

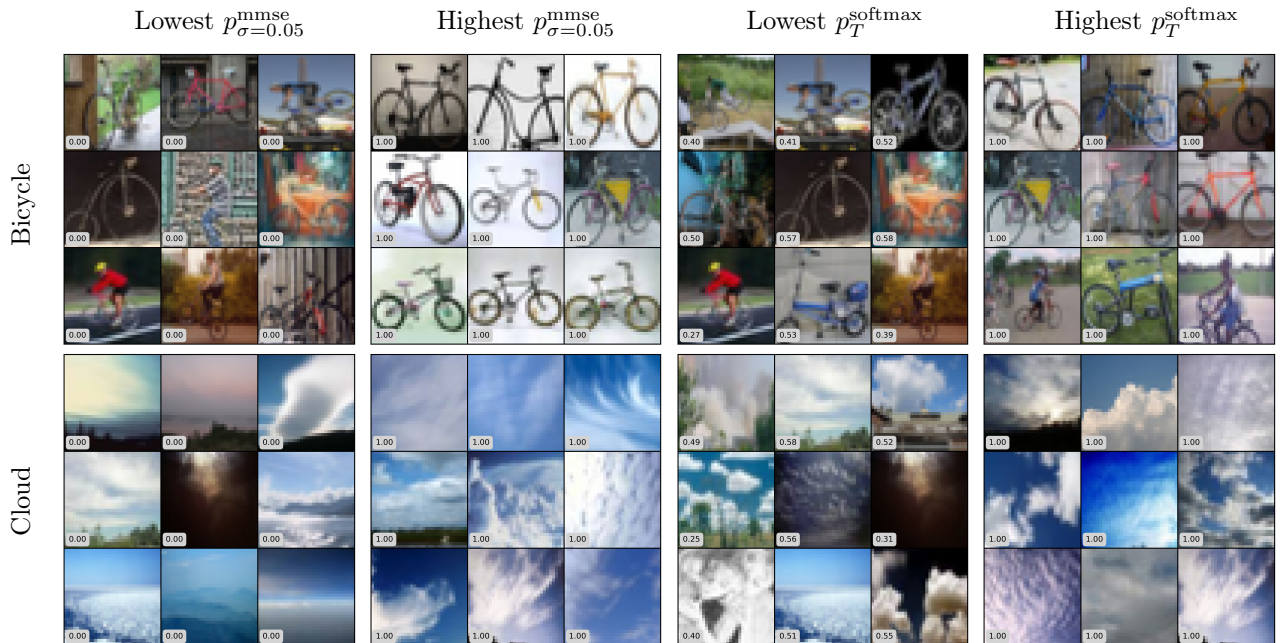


Figure 13: Images with the lowest and highest  $p_{\sigma}^{\text{robust}}$  and  $p_T^{\text{softmax}}$  values among CIFAR100 classes. Images with high  $p_{\sigma}^{\text{robust}}$  tend to be brighter and have stronger object-background contrast (making them more robust to random noise) than those with low  $p_{\sigma}^{\text{robust}}$ . The difference between images with high and low  $p_T^{\text{softmax}}$  is less clear. Thus,  $p_{\sigma}^{\text{robust}}$  better captures the model’s local robustness with respect to an input than  $p_T^{\text{softmax}}$ .

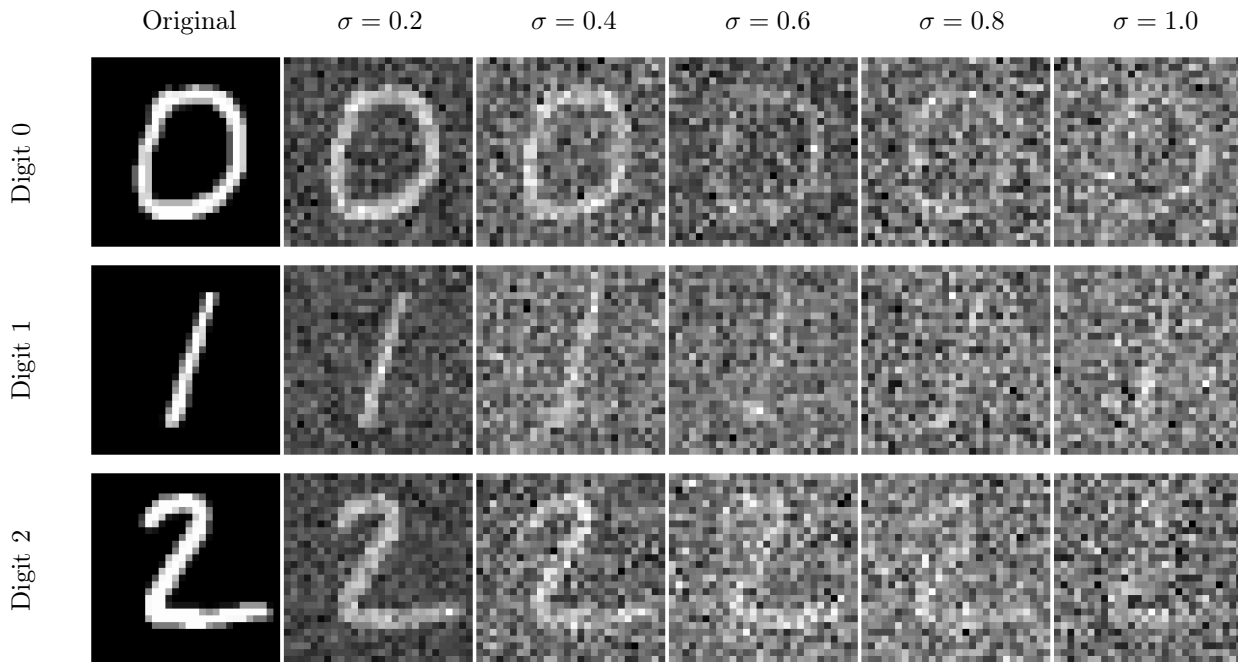


Figure 14: Examples of noisy images for MNIST.

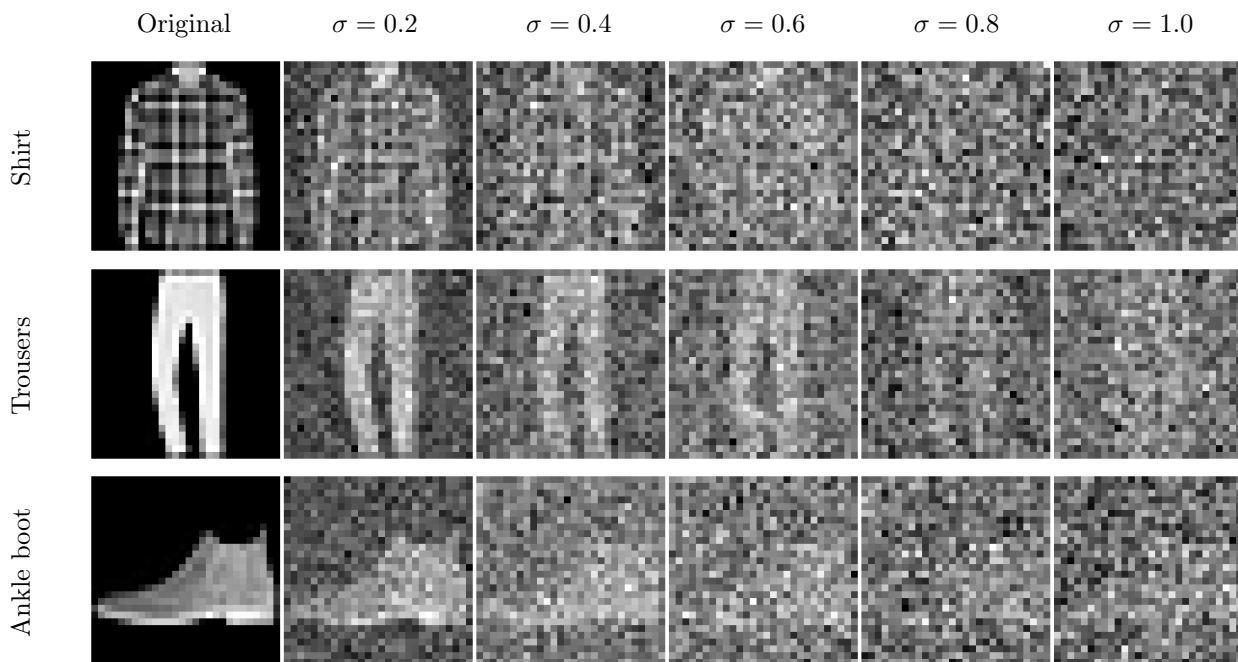


Figure 15: Examples of noisy images for FMNIST.

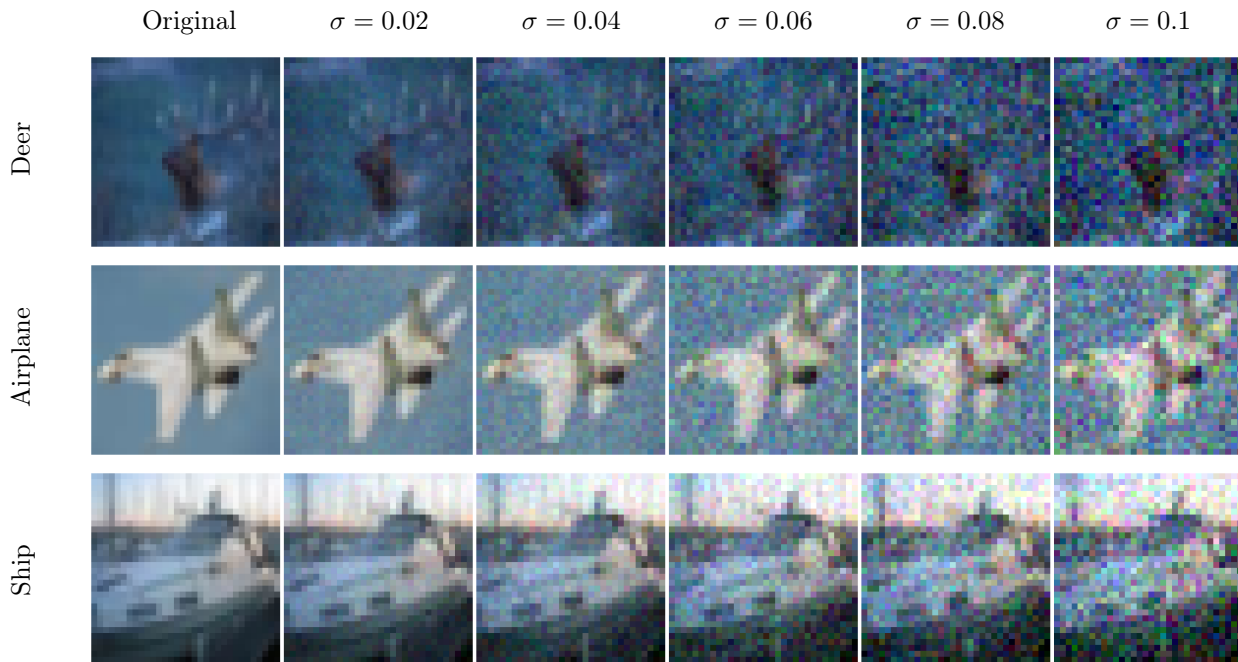


Figure 16: Examples of noisy images for CIFAR10.

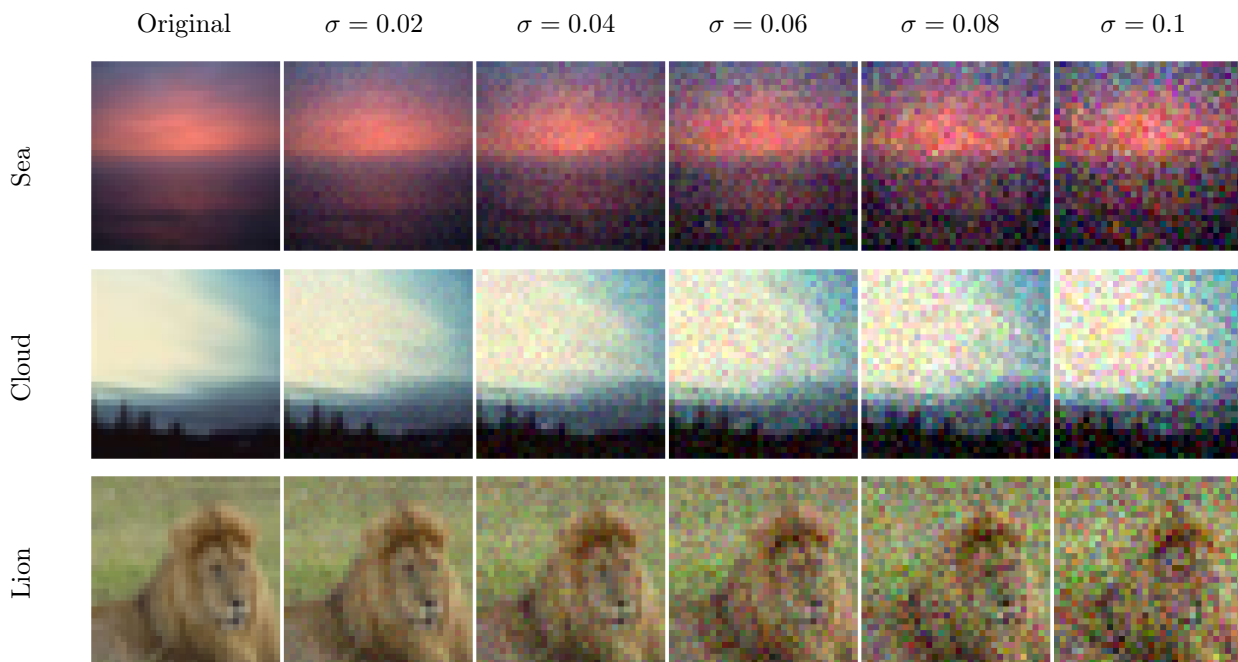


Figure 17: Examples of noisy images for CIFAR100.